Development of a 18F-labelled carborane-peptide conjugate for Boron neutron capture therapy (BNCT)

Master`s thesis

Master`s degree program in Chemistry of Drug development

Radiopharmaceutical chemistry

Department of chemistry

University of Turku

Asanka Madubashini Narangoda

29.05.2026

Turku

The originality of this thesis has been checked in accordance with the University of Turku quality assurance system using the Turnitin Originality Check service.

Master´s thesis, University of Turku, Turku, Finland
Chemistry of Drug Development: Radiopharmaceutical Chemistry
Author: Asanka Madubashini Narangoda
Tittle: Development of a 18F-labelled carborane-peptide conjugate for boron neutron capture therapy (BNCT)
Supervisor: Professor Anu J. Airaksinen, PhD
Number of pages: 64
Date: 29.05.2026

Abstract

Brain tumors are heterogeneous group of neoplasms that could arise within the brain and are associated with considerable morbidity and mortality, due to unregulated cellular proliferation, aggressive biological behavior, and significantly resistant to conventional treatments. Blood brain barrier (BBB) is one of a major challenge which substantially restrict or prevent the delivery of many diagnostic and chemotherapeutic agents to the central nervous system. Boron neutron capture therapy (BNCT) is a targeted therapeutic strategy that based on the selective accumulation of boron-10 compounds in the tumor cells. In this research the boron delivery agent is FNA-S-ACooP which is a novel peptide-based radiotracer and also binding to $FABP_3$ (fatty acid binding protein).The aim of this research was to develop a novel boron carrier, based on the ACooP (H-ACGLSGLGVA-NH_2) a linear decapeptide and which can be radiolabelled with fluorine-18 for diagnostic purposes. In parallel, ACooP is a brain tumour homing peptide and is recognized for fatty acid binding protein as well as mammary derived growth -inhibitor.

In this research, FNA-S-ACooP and the carborane moiety contributes significantly as all the conjugations are based on this carborane-peptide scaffold structure. In the synthesis of FNA-S-ACooP fluoronicotinic acid-4-nitrophenyl ester serves as the prosthetic group which has a high ability of conjugating with numerous biomolecules due to presence of activated ester. Previous investigations revealed that all published reports related to conjugations between FNA, and biomolecules indicated N acylated derivatives except the conjugation with AcooP peptide. Therefore, as the first step of the reaction scheme it was successfully synthesis and characterized FNA-S-ACooP. The reaction was carried out under borate buffer with 70% of acetonitrile under 8.3 pH for 10 min and yielded FNA-S-ACooP with 62.3 %.

The initial approach was direct carborane-peptide conjugation, but unfortunately the reaction did not result and unable to characterized to correct product. As the second approach it was decided to investigate conjugation of the carborane to the peptide by using a PEGylated linker. FNA-S-ACooP was first reacted with Azido-PEG-NHS-ester to give FNA-S-ACooP-N-PEG_2-N_3. Upon the first attempt it resulted product, but it was observed that the conjugation efficiency has been mitigated, during the reaction. Therefore, to overcome this barrier it was required to enhance the accessibility of the active sites of the reactants. Simultaneously, it became evident that it is necessary of purifying the product and the reactants with formic acid over trifluoro acetic acid in order to enhance the accessibility of reaction sites. Following the modification

FNA-S-ACooP-N-PEG_2-N_3 yielded with 76.8 %. The subsequent step involved the integration of carborane moiety to the peptide back bone and eventually to synthesize the target compound carborane-N-FNA-S-ACooP with azido functionalized peptide via copper catalysed 1,3-dipolar cycloaddition. However, the incorporation of carborane cluster to propargyl-PEG_3-amine reaction was not able to be optimised under the investigated condition. Therefore, the intended compound which is carborane-N-FNA-S-ACooP was not able to achieve.

The synthesis procedure and the isolation and purification and characterization associated with considerable challenges. In conclusion, further optimization is needed in order to find optimal reaction conditions for conjugation of carborane to FNA-S-ACooP peptide.

Key words: FNA-S-ACooP, BNCT, carborane, PET imaging, fluorine-18,

Table of Contents

List of abbreviations

ACN	Acetonitrile
BBB	Blood brain barrier
BNCT	Boron neutron capture therapy
CNS	Central nervous system
CT	Computed tomography
FNA	Fluoro nicotinic acid-4-nitrophenyl ester
HCOOH	Formic acid
HRMS	High resolution mass spectrometry
HSQC	Hetero Nuclear single quantum coherence
MALDI	Matrix assisted laser desorption ionisation
MRI	Magnetic resonance imaging
NMR	Nuclear magnetic resonance
QC	Quality control
RP-HPLC	Reverse phase- High performance liquid chromatography
TOCSY	Total correlation spectroscopy
TOF	Time of flight
PEG	Polyethylene glycol
PET	Positron emission tomography

1 Introduction

Brain cancers are so called unregulated cellular proliferations which occur specially in the brain and the central nervous system (CNS). It is one of the most difficult malignancies in oncology to treat due to highly aggressive biological behaviour, limited therapeutic responsiveness, critical anatomical location and invasive at the cellular level. The brain tumours can be classified as primary brain tumours and secondary brain tumours according to where they derived [1]. Therefore, the primary brain tumours are originating from the neural or glial cells of the brain whereas the secondary tumours that spread or metastasize from systemic cancers, originated in other organs like lungs and breast and propagate to the brain. Brain tumours are relatively uncommon compared to other malignancies and they contribute disproportionately cancer attributable complications and mortality. According to the global cancer statistics stated by the International Agency for Research and Cancer (IARC) [2] it has been observed in poor outcomes in high grade malignancies from the tumours of the brain and central nervous system and it has become a significant number of death worldwide.

Blood brain barrier (BBB)[3] is one of the major obstacles in the treatment of brain malignancies. This acts as a protective barrier and highly sensitive physiological interface that prevents or restricts the penetration of many systemic chemotherapeutic agents into the CNS. Concurrently, it also prevents entering the chemotherapy drugs from accessing the tumour. Moreover, gliomas are highly infiltrative in nature which limits complete surgical eradication. On the other hand, tumour molecular heterogeneity which makes them more resistant to treatments. The factors outlined, collectively limit the effectiveness of conventional therapies and clearly indicate the necessity for targeted and personalized treatment approaches. [4]

Recently, there was a substantial progress in understanding the molecular landscape of CSN tumours, giving rise to the development of the targeted therapies, personalized medicine approaches as well as specific molecular changes in tumour cells. Particularly, Positron Emission Tomography (PET) have enhanced diagnostic precision and improve diagnosis and allow better monitoring of treatment response. Beyond that, approaches such as targeted nuclide therapy and molecular imaging agents offer promising and prospective avenues for improving therapeutic selectivity and aim to deliver radiation directly to tumour cells and while minimizing damage to healthy tissues. These novel approaches and innovations are particularly relevant in the context of drug development and radio pharmaceutical research where specific tumour biomarkers can be used for both imaging and therapy.

Boron Neutron Capture Therapy (BNCT) is a special cancer treatment that specifically targets and destroys tumour cells very precisely and BNCT has been studied for therapeutic intervention of brain tumours over a decade for many cases [5–8].BNCT makes use of ^{10}B enriched compounds accumulating in tumour tissue and followed by irradiation with thermal neutrons to exert lethal effects on it without harming the nearby healthy brain tissues. PET imaging plays a pivotal role in BNCT providing a non-invasive method to assess boron uptake in tumours prior to neutron irradiation enabling optimize treatment planning and patient selection. In general, classic PET traces like ^{18}F-BPA are used to measure boron uptake in the tumour. Simultaneously, peptide-based PET tracers have emerged as promising candidate for PET imaging. The aim

of developing these peptide-based PET tracers is to develop tracers for visualizing tumour biology more extensively and improve BNCT targeting. For example, 18F-FNA-S-ACooP is a novel radio labelled peptide as well as a brain tumour homing peptide, optimised to bind fatty acid binding protein 3 (FABP3) illustrating specific binding to malignant tissues and indicating the feasibility of peptide tracers in targeted imaging of tumour phenotypes. Hence it reveals exactly where the tumour is and how it behaves. Through the use of these, medical professionals can improve BNCT treatments and ultimately advance of the theranostic strategies in cancer treatments.

2 Review of the literature

2.1 Positron Emission Tomography

Positron Emission Tomography (PET) is a non-invasive imaging technique in nuclear medicine facilitating the visualisation and quantification of physiological and molecular processes in vivo. PET imaging is mostly applied to identify cancer, infection, inflammation as well as neurological and cardiological imaging on the body according to the detection of radiation by the radiotracer. Radiotracers are the active biological molecules, labelled with radioisotope and aid in determining and measuring visually the physiological, biochemical or molecular processes withing the body using nuclear imaging modalities such as PET or SPECT. Within all tomographic approaches PET offers highest qualities of sensitivity and quantitative accuracy. Therefore, PET imaging is useful for both diagnostic and research purposes. PET detection systems complement to other imaging modalities for biological analyses such as computed tomography (CT) or magnetic resonance imaging (MRI). Hence combining PET with CT or MRI enables precise localization of tumour activity within the body and it induces diagnostic improvement, treatment planning and monitoring.

In PET imaging, there are several short-lived positron emitting radionuclides[9], that can be associate with biologically active molecules to form radio tracers. Some of the most common PET radionuclides can be considered as fluorine-18, oxygen-15, carbon-11 and gallium-68. The applications of these radionuclides in radiopharmaceutical synthesis mainly determined by their physical half-life and the method of production. For an instant fluorine-18 has a half-life of approximately 109.8 minutes and is produced by proton bombardment of oxygen-18 enriched water providing adequate time for multistep radiochemical synthesis. Hence the nuclear reaction is ^{18}O (p, n)^{18}F and this can be acquired by acceleration of proton in a cyclotron followed by an irradiation of targeted oxygen oxygen-18 enriched water. During the nuclear reaction it releases a neutron in the form of neutron beam radiation and leads to the formation of [^{18}F]fluoride. The most common PET radio tracer is [18F]fluorodeoxyglucose ([18F]FDG) which is a glucose analogue in which the hydroxyl group at the C-2 position (2-deoxy-2-[18F]fluoro-β-*D*-glucose) has been replace by 18F. [10,11]

Alternatively, the other nuclides possess significant shorter half-lives hence required onsite cyclotron production and rapid synthesis protocols for example Carbon-11 (20.4 min), Nitrogen-13 (9.97 min) and

Oxygen-15 (2.03 min). With Galium-68 it is possible to produce without a particle accelerator in a radionuclide generator and can be conveniently obtain from 68Ge/68Ga generator system with a half-life of about 68 minutes. The radio isotopes are typically produced on the same day they are used for clinical imaging, because PET radioisotopes have comparatively short half-lives.

The principle of PET imaging is based on β^+ decay which is so called positron emission by a radioisotope that is neutron deficient. A proton with the unstable nucleus is converted into a neutron during radioactive decay releasing a positron and a neutrino. Before interacting with an electron, the emitted positron travels a short distance in the tissue depending on its energy approximately 1-2 mm. This interaction results in a phenomenon called annihilation. Positron and the electron are destroyed during this annihilation and their masses transformed into energy in the form of two gamma photons. These photos are emitted concurrently to opposite direction approximately 180^0 apart. Each possess energy of 511 keV [12] which is equivalent to the mass of the electron or a positron as demonstrated in Einstein's mass-energy equivalence principle $E = mc^2$ [13] as well as accordance with conservation of momentum.

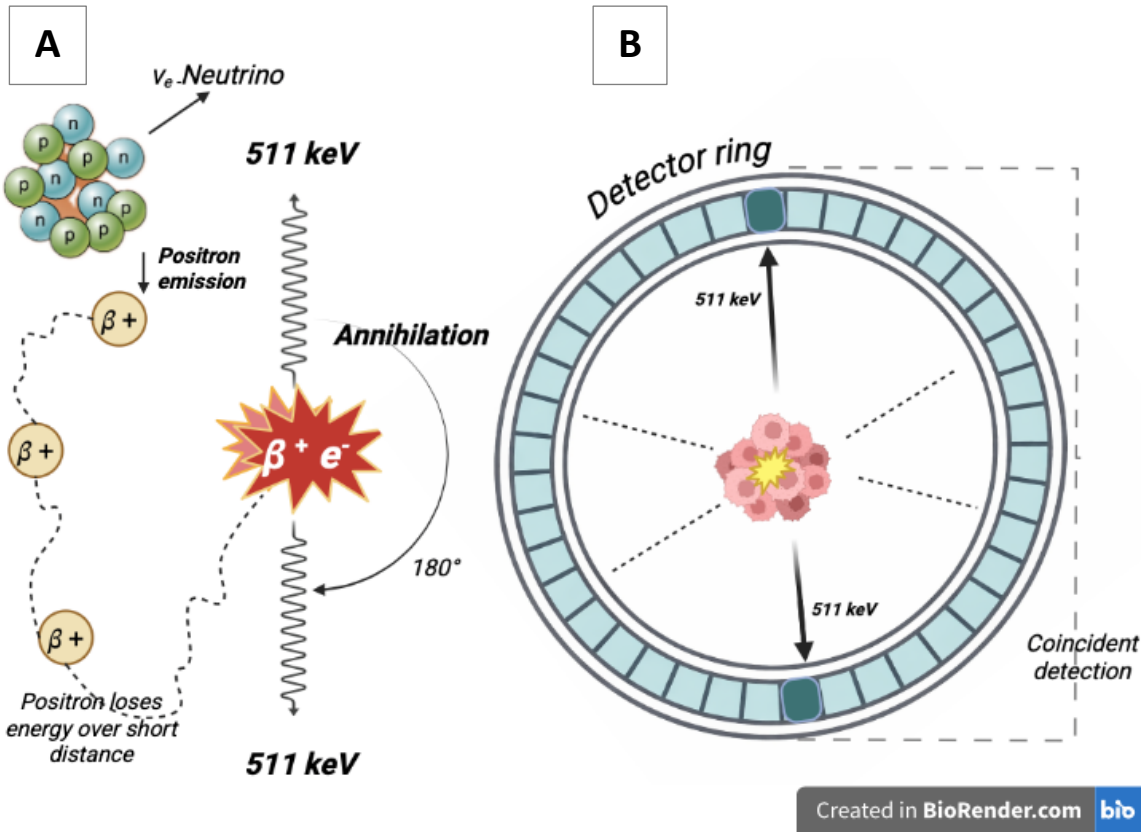

Figure 1: *Basic principle of PET imaging. The figure was adapted from*[14] [15] *and created with BioRender.com*.

Positron emitting radioisotopes are proton rich and exhibit intrinsic instability. Through the radioactive disintegration they acquired stable ground state while transforming a proton(p) within the nucleus into neutron (n) and a neutrino as depicted in Figure 1(A).

The core of the above illustrated diagram also be expressed by the following equation (1). X and Y represent the relevant element, atomic number denoted by Z and the mass number denoted by A.

Synchronous emission of proton with $180^0 \pm 0.25^0$ angle due to annihilation reaction between the positron and the electrons what makes PET imaging possible.

The PET scanner consists of ring shape arrangement comprising arrays of scintillation crystals adjoin to photodetectors. The scintillation materials have changed over a time; the most recent scintillators made of lutetium oxyorthosilicate (LSO) or utetium yttrium oxyorthosilicate (LYSO) whereas the old scintillators are consisting of bismuth germinate (BGO) and all of these are incorporate with highly sensitive photo sensors. The modern scintillators possess higher density, faster response time, and better energy resolution and, they are adjoining to highly sensitive photo sensors to improve PET imaging quality and detection efficiency. The detectors are designed to determine the coincidence detection of simultaneous 511 keV gamma rays and the localization of the annihilation points. Line of response (LOR) defined by the points of interaction with the detector array which the annihilation occurs. The location of single annihilation event occurred cannot be precisely determined, yet the collection of millions of coincident events permits computational reconstruction of the special distribution of the radiopharmaceutical. Positron range is defined by the distance travelled by the positron before annihilation, and it makes subtle effect in special resolution. PET scanners predominantly use coincident window of 6-12 nano seconds to make sure that only proton from the same annihilation event are recorded to mitigate the background noise. This principle supports the high density of PET detecting molecular processes in vivo enabling it a powerful tool for imaging, assessing therapeutic responses and navigating to the radiopharmaceutical development.[16]

2.2 Potential drawbacks of the coincidence detection techniques in PET scanner.

It is true that coincidence detection forms the fundamental principle of positron emission tomography (PET). Yet there are several facts including physical and instrumental factors which may affect and limit the accuracy and special resolution of the techniques. Optimally, PET scanners should record only true coincident events, which occur when two 511 keV photons generated from a single annihilation are detected concurrently by two opposing detectors. The line of response (LOR) is defined by these protons by traveling nearly opposite directions, across this the annihilation even is assumed to have occurred. In reality, not all the detected events are correlated with true coincidences, and the several factors cause ambiguities and weaken the image quality.[17]

In fact, the random coincidence events develop the major limitations. This happens when two photons originating from different annihilations events are detected within the coincident time window and are erroneously recorded as a reliable coincidence pair. As the photons do not originate from the same annihilation even there's no correspond of designated LOR to the precise location of the radiotracer distribution. Therefore, random coincidences create statistical noise and lower the signal to noise ratio of PET images. With higher activity levels and wider coincident time windows the probability of random events increases leading them a significant source of background in PET imaging[16].

Figure 2: *Random coincidence of PET scanning:* ***(i)*** *True coincidence event;* ***(ii)*** *Random Coincidence; (iii) misposition of coincidence event. Adapted by Shukla AK, Kumar U. Positron emission tomography: An overview. J Med Phys. 2006 Jan;31(1):13-21. doi: 10.4103/0971-6203.25665. PMID: 21206635; PMCID: PMC3003889.*

Scatter coincident event is another important source of error which describe one or both annihilation Compton scattering within the patience body before reaching the detector. This scattering outlines the changes of direction and energy of photons resulting them to be incorrectly assigned to an LOR that does not align with the exact annihilation location. Scatter event may represent a considerable fraction of the recorded coincidences it may create low image contrast and inaccurate quantification of tracer uptake. Even though the complete elimination of scattered photons is not possible the energy discrimination techniques are using to reduce the effects.

Fundamental physical effects related with positron emission tomography limits the PET spatial resolution. Positron range is one such factor associates with the distance travelled by an emitted positron before it losses its kinetic energy and annihilates with an electron. In contrast to the site of radioactive decay PET imaging detects the location of the annihilation, therefore the detected position may be slightly shifted from the origin of the radiotracer. The degree or the magnitude of this effect is influenced by the kinetic energy of the emitted positron, hence varying among different radionuclides.[18]

Proton a collinearity is another inherent drawback in PET imaging. In principle two annihilated protons are emitted exactly 180^0 apart. Since the positron electron pair may still retain residual momentum at the time of annihilation the photons are emitted at slightly altered angles. In most cases diverging by proximately $\pm$ 0.2^0. This small angular deviation leads to uncertainty in the restored LOR, especially in scanners with large detector ring diameters, hence slightly diminishing the special resolution.[19]

Apart of these physical drawbacks detector and system characteristics can also be an impact for coincidence detection. Limited time resolution, limited detector efficiency and high-count rates may result multiple coincident events. This occurs when more than two detectors register signals with the coincidence time window. Such ambivalent events are generally eliminated as it directly effects to reduce the overall sensitivity of the scanner. Moreover, a substantial proportion of detected photons are single events, whereas only one photon of the annihilation pair is detected, giving rise to a significant loss of potentially beneficial data[20].Collectively, although the coincidence detection empowers PET to provide highly sensitive molecular imaging its execution is influence by several physical effects and substandard detection events.

Developed correlation algorithms improve detector technologies and time of flights PET systems are thus used to minimize these limitations and optimize image quality.

2.3 Evolution of Positron Emission Tomography

Positron emission tomography (PET) has evolved into one of the most powerful molecular imaging techniques for studying biological processes in vivo and for evaluating novel radiopharmaceuticals. Since its early development in the mid-20th century, PET has progressed from an experimental nuclear imaging concept into a clinically indispensable modality capable of providing quantitative information on metabolism, receptor binding, and tracer biodistribution throughout the body. The ability to track radiolabelled compounds at extremely low concentrations has made PET particularly valuable in the development and validation of new molecular imaging probes, including fluorine-18 labelled tracers used in oncology, neurology, and therapy planning. [21,22]The conceptual foundation of PET imaging emerged in the 1950s and 1960s, when early positron detection systems were developed based on coincidence detection principles. These early instruments laid the groundwork for tomographic imaging, but it was not until the 1970s that practical PET scanners began to appear with ring-based detector geometries and computational reconstruction algorithms that allowed cross-sectional imaging of radiotracer distributions. The following decades witnessed rapid technological improvements in detector materials, electronics, and computational capabilities. These advances significantly improved spatial resolution, sensitivity, and quantitative accuracy, transforming PET from a primarily research-oriented tool into a clinically viable imaging modality.

A major milestone in the clinical expansion of PET was the introduction of hybrid imaging systems. The integration of PET with computed tomography (PET/CT) in the late 1990s allowed simultaneous acquisition of functional and anatomical information, improving lesion localization and enabling more accurate attenuation correction [23]. PET/CT rapidly became the standard clinical platform, particularly in oncological imaging where metabolic information from PET complements structural information from CT. Later developments introduced PET/MRI systems, which combine molecular imaging with high soft-tissue contrast and reduced radiation exposure, expanding the applications of PET in neurological and pediatric imaging.

Another important technological advancement in PET instrumentation was the implementation of time-of-flight (TOF) reconstruction techniques. By incorporating precise timing information into the reconstruction process, TOF PET significantly improves signal-to-noise ratio and image quality, particularly in large patients or low-count imaging conditions [24]. The introduction of TOF capabilities, together with improvements in detector crystals and photodetector technologies such as silicon photomultipliers, further enhanced PET sensitivity and quantitative performance.More recently, the development of long axial field-of-view (LAFOV) and total-body PET scanners has marked a new era in molecular imaging. Unlike conventional PET systems that acquire images sequentially across multiple bed positions, total-body PET

scanners extend detector coverage across a large portion or the entire human body, enabling simultaneous imaging of multiple organs with dramatically increased sensitivity [25]. This increase in sensitivity allows lower injected radiotracer doses, faster acquisition times, and comprehensive dynamic imaging of tracer kinetics throughout the body. These capabilities are particularly valuable for radiopharmaceutical research, where whole-body pharmacokinetics and organ-to-organ tracer interactions can be studied in detail.

2.4 The quantitative measure of molar activity (A_m)

The molar activity (A_m) also referred to as specific activity[26] is a crucial factor in radiopharmaceutical chemistry that quantifies the radioactivity associated with a specific amount of compound. It is the activity of the radiolabelled compound per mole of the molecule by the definition and generally expressed with GBq/μmol. PET tracers required high molar activity to acheive optimal imaging performance because it ensures that the administrated tracer dose contains trivial amount of non-radioactive compound or the cold compound. Otherwise, it causes the saturation of biological target and reduces imaging sensitivity or therapeutic performance.[27]

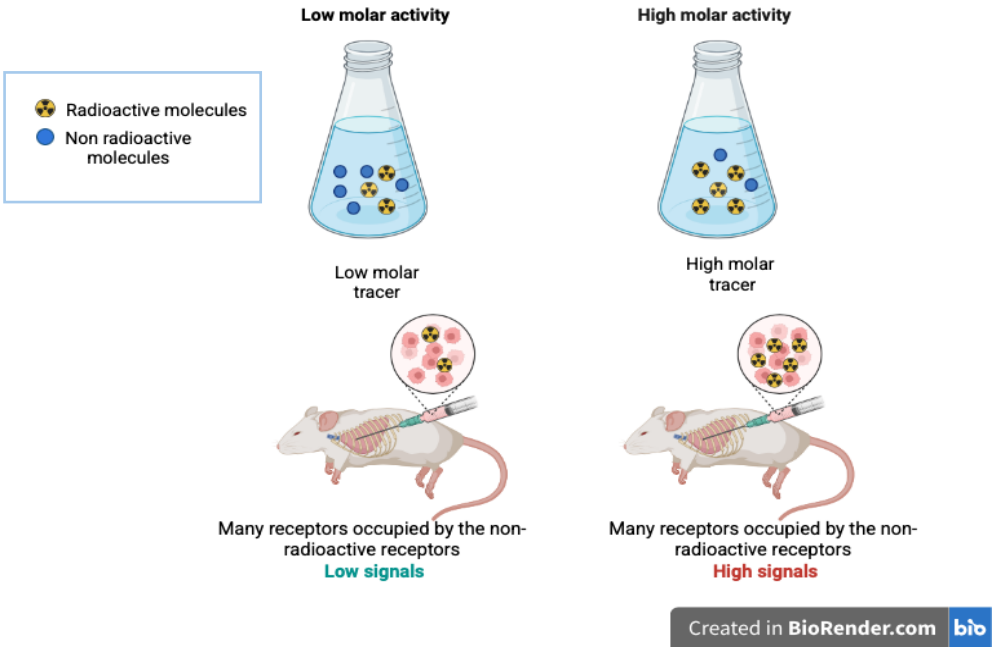

Figure 3: *Diagrammatical illustration of the concept of molar activity and how it affects the image resolution*

By measuring the total radioactivity of a purified radiotracer and calculating the equivalent molar concentration of the compound the molar activity can be determined experimentally. For instance, the half-life of fluorine -18 is approximately 110 min and for positron emitting tracers like 18F labelled peptides the decay of fluorine -18 must be considered and correction for radioactive decay are applied during measurements, to obtain the time correction at the end of synthesis (EOS). Presence of carrier fluoride during radiolabelling, poor labelling, or isotopic dilution during synthesis and purification can result to low molar activity and can have strong impact on imaging accuracy and receptor occupancy. On the other hand,

extremely high molar activity enhances relative contrast of target to background, especially high affinity molecular targets detected at low density, particularly certain peptides or antibodies in oncological PET imaging.

Therefore, it is necessary to control molar activity in PET tracer development to make sure reliable imaging results and for maintaining safety in preclinical or clinical applications. In order to quantifying the radiolabelled fraction, it is possible to use radio HPLC which is a standard method for determining A_m. To determine the total mass, it is possible to use UV or mass spectrometry, and it allows accurate calculation of radioactivity per mole of tracer. Accurate reporting of A_m [28]is very important in publication as it enables reproducibility and comparison of tracer performance across different studies and laboratories.[29]

2.5 Peptide based PET radiopharmaceuticals

Due to the high selectivity or affinity towards specific biological targets peptide-based radiopharmaceuticals have become an important group of molecular imaging agents in nuclear medicine. To visualise or monitor the biochemical processes using imaging modalities such as PET these radiotracers are designed by coupling targeting peptide with a radioactive isotope. Peptides can exhibit favourable properties such as high receptor affinity, favourable pharmacokinetics and rapid systematic elimination of target tissues making them attractive candidate for radiopharmaceutical application. Further, they are attractive and desirable targeting vectors yielding to high target to background contrast. Recently, the development of fluorine-18 labelled peptide radiopharmaceuticals has acquired a significant attention in diagnostic imaging and prospective therapeutic applications.[30]

The ability to bind selectively to the receptors that are upregulated in diseased tissues specially in cancer is a significant benefit of peptide-based radiopharmaceuticals. Tumours are frequently highly expressed peptide receptors as they contain few major receptors such as somatostatin receptors, integrins and bombesin receptors making them effective targets for peptide – based imaging agents. Highly specific and selective radiotracers can be developed by designing peptide that specifically identified these receptors for precise and accurate disease detection and characterisation. In this case, it is critical to understand the concept of pharmacophore. The pharmacophore illustrates the pivotal structural features of a molecule that facilitates with a specific biological target. During the radiotracer designing, performance and the enhancement of the pharmacophore is challenging while ensuring peptide to maintain its binding affinity and specificity even after chemical modification for radiolabelling.

Despite receptor targeting peptide-based radiopharmaceuticals can be modified to detect specific cancer biomarkers and adapted biological processes directly linked with tumour progression. Cancer biomarkers, overexpressed enzymes, growth factor receptors, and other tumour associated proteins provides promising targets for imaging. Peptides can be specifically designed to interact with these biomarkers, with strong selectivity permitting for the visualization of molecular changes that emerge during molecular development. For example, enzymes engaged in tumour growth and invasion can serve as indicators of malignancy and aggressiveness. Introducing effective pharmacophoric features into peptide structures

allows selective binding to such enzymatic targets while remaining and preserving biological activity. Moreover, to determine fundamental biological processes such as energy metabolism which is often disrupted in cancer cells can be determined by peptide-based PET- tracers. Tumour cells illustrate metabolic alteration which includes glucose uptake and restructuring metabolic pathways to sustain accelerated proliferation. Particularly, radiopharmaceuticals labelled with fluorine-18 are beneficial for monitoring these metabolic alterations in vivo providing analytical insight into tumour physiology and treatment response. This bifunctional capacity of aiming both biomarkers and biological processes considerably develops the clinical relevance of peptide-based radiopharmaceuticals in personalized medicine.

Fluorine-18 is one of the most widely engaged radionuclides in PET imaging caused by its favourable physical and nuclear characteristics. The half-life of fluorine 18 is approximately 110 minutes which is adequately long enough to allow to multistep synthesis and imaging procedures while mitigating radiation exposure. On the other hand, it results a high-resolution energy due to low positron energy. It is possible to produce fluorine 18 in large scales by the aid of a cyclotron and make them highly suitable for clinical purposes. In actual clinical settings, particularly in clinical imaging of cancer, neuroglical disorders, and cardiovascular diseases the role of fluorine 18 labelled tracers is broad as the application of them are highly advantageous.[30]

Regardless of these befits fluorine 18 radiolabelling of peptides is demanding as it requires harsh reaction conditions for the fluorination such as high temperatures and strong bases. These conditions are often not compatible with the sensitive structure of the peptide, and it may result in degradation or loss of biological function of the peptide. To address these challenges and limitations divergent approaches have been developed. One of a widely adopted strategy involves the use of a prosthetic group. Prosthetic group is a small molecule that can be 18F-labelled and subjected to conjugation with a peptide under a mild condition which helps to preserve the structural stability and biological activity of the peptide. N-succinimidyl-4-fluorobenzoate ([18F]SFB) are commonly used prosthetic groups for 18F labelling. [18F]SFB is ready to reacts with primary amine groups present in the biomolecules to form stable amide bond, thereby facilitating the radiolabelling of biomolecules.

Along with prosthetic group strategies there are other few approaches fluoride acceptor chemistry and click chemistry have been employed to enhance the radiolabelling efficiency. In fluoride acceptor strategy contains synthesis of stable complexes between fluorine 18 and elements such as aluminium, silicon or boron. Chelators like NOTA or NODA provide relatively simple and efficient labelling pathway for peptides particularly when synthesising aluminium-^{18}F complexes. These strategies have significantly improved the possibility of producing ^{18}F- labelled peptide for medical applications.[31]

A necessary step in the development of peptide-based radiopharmaceuticals is quite extensive biological evaluation prior to clinical use. To assure the maximum performance radiotracers undergo comprehensive in vivo and in vitro studies. In vitro experiments investigate receptor binding affinity, stability and cellular uptake whereas in vivo assesses in animal models provide information on biodistribution, pharmacokinetics, metabolic stability and tumour targeting efficiency. It is important to understand the

tracer behaviour in vivo evaluations, specifically in complex biological systems, because some factors are directly affecting the imaging quality. Among those factors the major causes can be considered such as enzymatic degradation, plasma protein binding and non-specific organ uptake etc. To obtain a reliable diagnostic outcome it is necessary to optimize the parameters of those factors.

2.6 Cyclotron production of fluorine-18

Biomedical cyclotrons are mainly used to produce fluorine-18 through proton induced nuclear reactions and it is one of the most important radionuclides for PET. Widely implemented method of producing fluorine-18 is irradiation of enriched oxygen-18 (^{18}O) water targets via the ^{18}O (p, n)^{18}F reaction. In this reaction high energy beam of proton interacts with ^{18}O nucleus producing in the emission of neutron and the formation of ^{18}F. This reaction is generally carried out using proton energies in the range of 10- 20 MeV, enabling efficient production yield appropriate for clinical and research purposes [32]. As the target material it is necessary to use highly enriched [^{18}O]H_2O for maximising production efficiency and to obtain high activity level of ^{18}F.

In this process the cyclotron act as a particle accelerator. The protons are the charged particles, and they are accelerated in a spiral trajectory driven by a magnetic field and an alternating electric field until they reached the optimal or targeted energy. These accelerated protons then delivered to the target material contained within an explicitly assigned target system competent of withstanding high radiation doses and thermal strain. Efficient temperature regulation and cooling systems are critical components of the target set up to sustain stability during radiation [33]. As a result of bombardment fluorine-18 is produced in the form of aqueous [^{18}F] ions which is highly suitable for nucleophilic radiolabelling reactions.

Subsequent to radiation, the generated ^{18}F should be separated and purified before it can be utilised by the radiopharmaceutical synthesis. Generally, the irradiated target solution is transferred to processing system where [^{18}F]fluoride ions are trapped on an ion exchange resin. This facilitates separation from the enriched water and the other impurities after which the ^{18}F is eluted using standard eluents, widely used containing carbonate salt and phase transfer catalysts. The yielded no carrier added [^{18}F]fluoride demonstrates high molar activities, which is particularly important for receptor targeted imaging applications to avoid receptor saturation with minimal mass required.

Along with the production of nucleophilic [^{18}F] fluoride alternative synthesis routes can result electrophilic [^{18}F]fluorine gas, generally via radiation of gaseous $^{18}O_2$ or through secondary processing methods. However, due to the presence of carrier fluorine-19 the electrophilic fluorine generally exhibits lower molar activities [34]. Thus, nucleophilic [^{18}F] fluoride could be considered as the preferred form for most radiopharmaceutical synthesis particularly in peptide-based tracer development.[35]

The cyclotron production of ^{18}F has advantages, among which are reproducibility, high yield and the ability to produce the radionuclide in large scales suitable for pre-clinical and even for routine clinical use. The production batches could be containing hundreds of giga-becquerels of activity, which could be utilised for

preparation of many patients doses from a single production run[33]. In addition to this, it is required the close distance between the cyclotron facilities and imaging centre as it is necessary to carried out the synthesis rapidly, quality control, and distribution of ^{18}F-labelled radiopharmaceuticals, of which are having relatively short half-lives (approximately 110 minutes).

Comprehensively, cyclotron-based production of fluorine-18 is a widely recognised and well established and highly efficient process which sustains the widespread use of PET imaging in modern nuclear medicine. It assures the robust supply of high purity ^{18}F for radiopharmaceutical applications by optimising the nuclear reaction developed and high-level target systems as well as efficient purification techniques. This production techniques are very crucial in empowering the translation of novel imaging agents into real medicine, detecting accurate disease diagnostic monitoring and personalised treatment plans.

2.7 Activated esters of fluoro nicotinic acid as 18F prosthetic groups

Activated esters of fluor nicotinic acid extracted from 6-[^{18}F] fluoronicotinic acid ([^{18}F]FNA). In positron emission tomography (PET) FNA has been recognised as immensely valuable prosthetic group for radiolabelling of biomolecules. Even though they are very important they have significant challenges in radiopharmaceutical chemistry. The challenges are including efficient labelling, in vivo stability, and compatibility with biological targeted vectors.

A core advancement of in this field is the development of activated esters such as [^{18}F]FNA 4-nitrophenyl ester, which contribute highly effective conjugation with biomolecules via N -acylation as well as S acylation reactions. [^{18}F]FNA provides straightforward and reliable radiosynthesis. Particularly, the synthesis procedure could be achieved through nucleophilic substitution. Therefore, the advancement of automation potential and the reproducibility has been accomplished by using K[^{18}F]F/Kryptofix chemistry or via on resin fluorination and avoiding work intensive steps such as azeotropic drying[36].

Diversity of adaptability of [^{18}F]FNA esters have been proven through their successful application in conjugating diverse biomolecules. Although activated esters of fluoronicotinic acid have been successfully used for radiolabelling biomolecules, rapid cleavage has been reported for certain N-acylated peptides conjugates[37]. The activated ester reacts with amino functionalised folate derivatives as well. Even though the reaction conditions may differ based on the biomolecule, [^{18}F]FNA-folate radioconjugate process highlights both efficient and adaptability of [^{18}F]FNA chemistry. Generally the peptide conjugation progresses under mild conditions, folate conjugation requires optimization using organic basses such as triethyl amine in dimethyl sulphoxide to achieve sufficient yield[36]. This conforms; the reactivity of activated esters can be affected by the chemical environment and the functional group accessibility of the target molecule.

From the biological point of view [^{18}F]FNA based conjugates shows significant in vivo stability which is a vital requirement in for PET imaging. However recent studies have reported rapid cleavage in N acylated ACooP peptide conjugate reveal potential limitations in the stability of certain [^{18}F]FNA derived radio

conjugates. In this [^{18}F]FNA-folate, more than 95% of the tracer remain unchanged in circulation after 60 minutes illustrate minimum radio metabolism and reliable quantification of PET signals [36].In addition, low bone uptake shows minimal or negligible defluorination, and strengthening the stability of the C-F bond in the system. These characteristics are crucial for accurate imaging and prove the viability of [^{18}F]FNA for clinical approaches.

Besides the conjugated systems, the parent compound [^{18}F]FNA itself has also been evaluated as a PET tracer, especially in the context of glioblastoma imaging. This work highlights that [^{18}F]FNA can employ as monocarboxylate transporter 1 (MCT 1) to penetrate the blood brain barrier (BBB), facilitating visualization of brain tumours. Most importantly, tumour uptake was significantly mitigated upon MCT 1 inhibition which is verifying transporter mediated uptake mechanism [38]. This observation not only collaborated the biological relevance of fluoronicotinic acid derivatives but also confirms that [^{18}F]FNA based prosthetic group may sustain or contribute functional targeting properties depending on their molecular context. Another major advantage of fluorine-18 labelling is its physical half- life 109.7 min which enables for extended imaging protocol and transport to remote clinical sites. When compared to the carbon-11 labelled analogues which are limited to short life approximately 20 minutes, the fluorine-18 shows a significant improvement [38]. Hence, [^{18}F]FNA- based prosthetic groups are suitable for regular clinical use with certain limitations.The applications of activated [^{18}F]FNA esters also immensely contribute for the advancement of theranostic agents. By making the ground for the efficient conjugation to peptide, antibodies and small molecules these prosthetic groups enable the design of targeted imaging agent that can likely to be align with the therapeutic analogues. As an example, [^{18}F]FNA conjugates have already validated clinically the applicability in clinically used tracers such as PSMA- targeting agent revealing their translational potential [36].

Regardless of the advantages mentioned there are some certain limitations retained. One key limitation is the efficiency of conjugate reactions could be varied due to the biomolecule further the radiolysis may take place in sensitive compounds such as folate derivatives and thus it requires the stabilizing additives such as ascorbic acid. In addition to this the biological behaviour of [^{18}F]FNA conjugates not only depends on the prosthetic group but also depends on the targeting moiety requiring optimised design and validation for each application. Activated esters of fluoronicotinic acid specifically [^{18}F]FNA- 4-nitrophenyl ester indicates a powerful and versatile category of prosthetic groups for ^{18}F radiolabelling. Their synthetic techniques indicate high reactivity, high effectiveness in vivo stability, and compatibility with diverse biomolecules make them suitable for PET imaging and theranostic enhancements. further research and developments for optimization and application of this field of studies are expected to advance molecular imaging, especially in oncology and inflammation areas.

2.8 Novel radiolabelled peptide FNA-S-ACooP

The development of novel peptide-based radiotracers has substantially progressed in targeted molecular imaging. Within this group, the fluorine-18 labelled peptide FNA-S-ACooP shows a promising result for targeting fatty acid binding protein (FABP3) a biomarker with clinical importance I n cancer. ACooP is a linear decapeptide consists of free amino group and a thiol functional group offering a platform for labelling due to presence of multiple reaction sites [5].The amino acid sequence of FNA-S-ACooP is reported as ACGLSGLGVA which consists of free N terminal amine and a cysteine residue containing a thiol functional group.

[^{18}F]FNA-S-ACooP consists of a prosthetic group which is 6-[^{18}F]fluoronicotinic acid-4-nitrophenyl ester. This activated ester provides efficient conjugation of fluorine-18 to the peptide under mild conditions. Remarkably, conversely to the expectation of N-acylation at the amino group, the conjugation occurred via S-acylation of the thiol group of the pepetide. This regioselectivity reaction proceeds to the formation of radiolabelled product [^{18}F]FNA-S-ACooP which the structural characterization has been carried out with analytical methods such as radio HPLC, NMR[5]. This observation is very important as its indicates that fluoronicotinic acid which is an acid base prosthetic group which could be shown unique reactivity depending on the biomolecule present in the molecule.

To obtain a better chemical yield approximately 30% and high chemical purity which is more than 96%, the radiosynthesis of the prosthetic group itself was synthesized using an efficient on -resin fluorination method. This methodology enables more straightforward synthesis process and facilitates the practical production of ^{18}F-labelled peptides research and possible clinical use [5].The obtained radiotracer was found to be hydrophilic, as suggested by its partition coefficient, largely favourable for biological distribution and clearance.

In vivo/ in vitro evaluations [^{18}F]FNA-S-ACooP has shown promising targeting results. Invitro autoradiography studies using human tumour tissue demonstrated heterogeneous but strong site-specific binding of the radiotracer in malignant region. Significantly, this binding aligned with the expression of FABP3, and this could be confirmed by immunofluorescence staining. Inhibition experiments can be carried out by using non labelled peptides considerably reduced tracer binding and this collaborates the specificity of [^{18}F]FNA-S-ACooP towards its intended target[5].These findings suggests the capacity of this radiolabelled peptide for targeted imaging of FABP3 expressing tumours.

Despite these notable results, it has been identified certain drawbacks as well. During the stability experiments it has been observed that [^{18}F]FNA-S-ACooP subjected to rapid metabolism oin plasma, with only a minimal fraction of intact tracer remaining after a short incubation period. This confirms that the peptide structure itself causes for the instability rather than the prosthetic group. Hence, further optimization of peptide sequences or structural modifications may be required to improve in vivo stability and develop imaging performances.

Development of [^{18}F]FNA-S-ACooP highlights the potential of fluoronicotinic acid- based prosthetic groups in peptide radiolabelling. This study contributes key insight into chemo selective conjugation, efficient

radiosynthesis and most importantly the target specific binding. It is required the patient-based evaluations and further pre-clinical validation studies regarding stability and pharmacokinetics, but this approach indicates an important milestone towards the development of novel peptide-based PET tracers for cancer imaging.

2.9 Boron neutron capture therapy (BNCT).

Boron neutron capture therapy is an advanced and sophisticated technique, and it is a combination of nuclear physics and targeted drug delivery. The treatment based upon dual approach, where two individually nontoxic components boron-10 (^{10}B) and a neutron beam associate to produce a localized therapeutic effect. Primarily, a boron containing compound is administrated and allow to aggregate preferentially within tumour cells. Subsequently followed by radiation with low energy neutrons such as thermal or epithermal. The disintegration of ^{10}B (nuclear reaction) triggers within boron loaded cell resulting in selective tumour destruction[39 40].

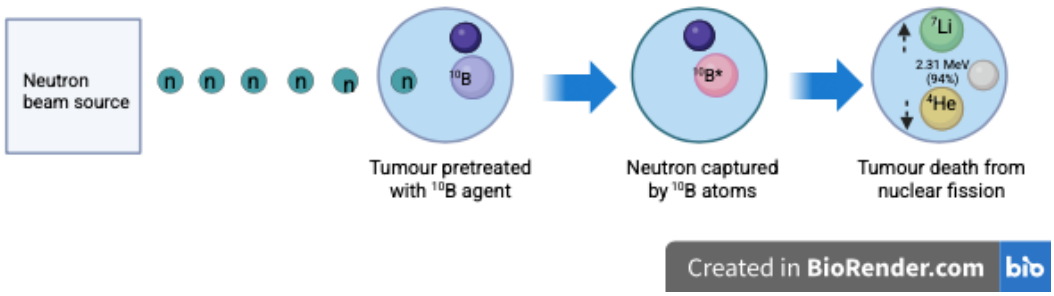

Figure3: *Schematic representation of tumour destruction by ^{10}B disintegration*

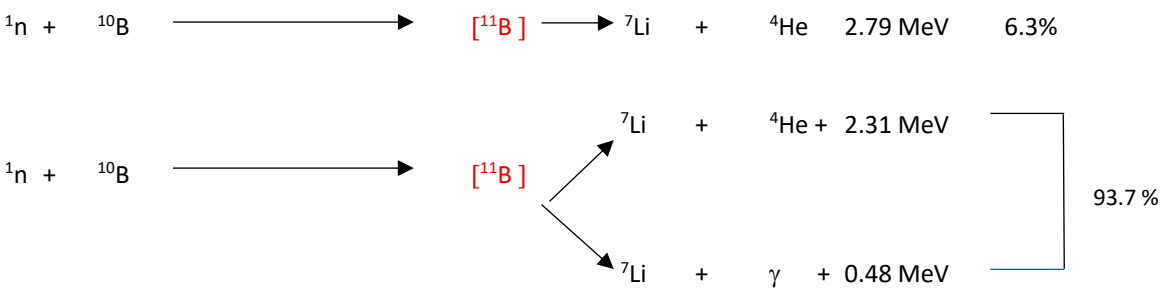

Figure 4: *The nuclear reaction of the boron atom. The dominant of which is accompanied by the production of high energy rays.*

The principal mechanism of BNCT includes the neutron capture reaction of ^{10}B generating an unstable intermediate ^{11}B that rapidly undergoes the process fission to produce high linear energy transfer (LET) particles which are alpha particles (^{4}He) and lithium-7 nuclei. Within a very short path length approximately 5-9 μm, these particles release a large amount of energy which is equivalent to the diameter of a single

cell. Consequently, the cytotoxic effect is strongly localised, allowing the destruction of boron containing tumour cells while largely sparing surrounding healthy tissues [40].

Cellular level selectivity is one of a major advantage of BNCT over conventional radiotherapy techniques. In general, external beam radiation deposits energy along its entire path where as BNCT relies on the preferential accumulation of boron in tumour cells. Therefore, during the neutron radiation only the tumour cells that are containing sufficient amount of boron are affected. This causes particularly favourable for treating infiltrative and recurrent tumours, such as glioblastoma, melanoma, and head and neck cancers, where conventional treatments often cause damage to normal tissues [41].

Efficient delivery and the retention of boron within tumour tissues highly matters for the success of BNCT. To accomplish the clinical benefits, it is required approximately 20-35 μg / g concentration of boron in the tumour tissue. Hence, favourable tumour to normal tissue (T/N) and tumour to blood (T/B) ratio preferably exceeding 3:1 ratio. Furthermore, boron agent should demonstrate low systematic toxicity and rapid clearance from normal tissues. In addition, currently available clinical agents such as boronophenylalanine (BPA) and sodiumborocaptate (BSH)[42], often demonstrate suboptimal selectivity and heterogeneous tumour uptake which mitigate treatment efficiency. [41].

Even though there were certain drawbacks, BNCT has several biological advantages as well. Generating high LET particles is characteristic in this therapy during the reaction and it is effective regardless of tumour oxygenation status and can damage cells in all phases of cell cycle, including radioresistant hypoxic or quiescent cells. This indicates and differentiates BNCT from conventional and chemotherapy, which often depend on oxygen availability and cell proliferation status. In addition, BNCT generally requires fewer treatment session and has proven reduced adverse effect [39].

In 1950, in early clinical trials BNCT has undergone several phases of developments, since its initial concepts in 1930[42]. Even though the results of early stages of development were limited by inadequate boron delivery, and toxicity issues evolution and advancement of boron chemistry, imaging techniques and neutron sources have resulted renewed interest in this therapy. Particularly, the advancement of accelerator based neutron sources and novel boron delivery systems, which are including peptides, nanoparticles, and antibody conjugates has significantly improved its clinical applicability [40].

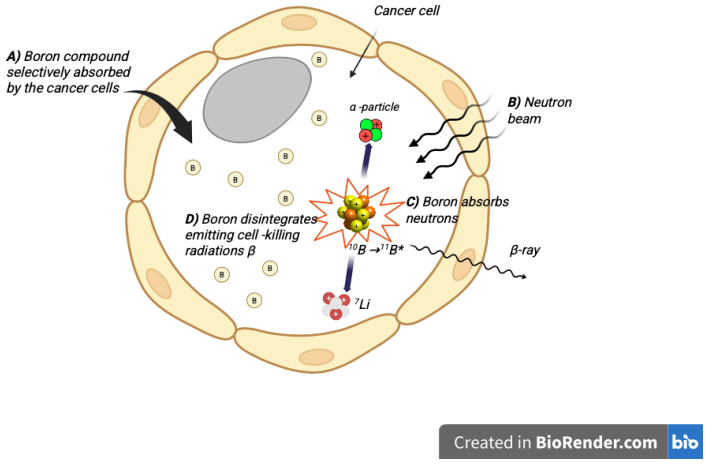

Figure 6: *Diagrammatic illustration of how BNCT functions within a tumour cell*

2.10 Carborane-peptide conjugation strategies

Carboranes are boron rich compounds which exhibit icosahedral cluster geometry. These carborane compounds have gained a considerable interest in the medicinal chemistry as they possess high boron content, chemical stability, and unique electronic structure. Carborane compounds are strongly hydrophobic and that character makes them particularly interesting as pharmacophores specifically in the development of boron delivery systems for boron neutron capture therapy. The poor aqueous solubility demands conjugation with biomolecules such as peptide to enhance their biological applicability [43].

Peptides are generally recognised as effective targeting vectors due to their ability of selectively bind to receptors that are overexpressed in tumour cells. This characteristic facilitates peptide-based systems to deliver therapeutic agents with greater specificity. Therefore, carborane-peptide conjugation reflects potentially effective approach to combine the high boron content of carborane with targeting ability of peptide, eventually improving tumour selectivity in BNCT applications [7]

One of the key approaches for synthesizing carborane-peptides conjugates is direct coupling. This could be achieved by using functionalized carborane derivatives such as Carborane-1-carboxylic acid. These compounds can be coupled to peptides via solid phase peptide synthesis (SPPS), where the carborane moiety is activated using coupling agents, for example HATU, COMU, or DIC/Oxyma) and the reaction proceed with nucleophilic site on the peptide. From the available functional group's primary amines such as the N-terminus or lysin sides chains have been recognised as the most efficient sites for conjugation and they generally form stable amide bonds with relatively high yields. Conversely, it has been revealed hydroxyl and thiol groups illustrate significantly lower reactivity resulting to poor coupling efficiency [43]

Even though the direct conjugation shows simplicity when reacting there are several limitations have been reported. The carborane clusters are bulky and highly hydrophobic in nature, this can be created steric hindrance and reduced accessibility to reactive sites on the peptide. Further, the electronic properties of the cluster can influence reactivity, resulting some conjugation reactions less efficient. These limitations often lead to incomplete reactions or insufficient yield, especially when complex peptide agents or sequence are involved in the reaction. On the other hand, the stability of different carborane isomers are implicated with meta and para carboranes generally performing better results compared to the more reactive ortho isomers[43].

To overcome these challenges linker-based strategies have been identified or developed. In order to provide flexible sufficient distance between the carborane cluster and the peptide, the use of spacer molecules, such as short organic linkers or polyethylene glycol (PEG) has been newly developed. This strategy mitigates the steric hindrance and enhances the overall efficiency of conjugation. In general, PEGylation is widely used to improve the physiochemical and biological properties of conjugation. The coupling of PEG chains can increases the water solubility, reduce accumulation and sustain circulation time in biological systems by improving stability and reducing fast clearance[44].

Additionally, to optimise synthetic efficiency, linker-based conjugation techniques also provide better control over the special arrangement of the carborane and peptide conjugation. On the other hand, it is

more important for biological applications where the distance between targeting peptide and the boron cluster can influence receptor binding and cellular uptake. A clear example for this is the incorporation of linker units such as glutaric acid or amino acid spacer has been observed to facilitate the synthesis of carborane containing peptide derivatives without compromising their targeting ability[45].

2.11 PEGylation strategies

PEG stands for polyethylene glycol and PEGylation contributes significantly for peptide bioconjugation chemistry as it plays an important role in developing the physiochemical and biological properties of peptide-based systems. The key purpose of employing this PEG is mainly to enhance the aqueous solubility and the molecular flexibility of the compound. There are few reasons why the PEGylation is more reliable method in radiopharmaceutical and therapeutic applications because, it contributes to reduce the peptide aggregation, withstand towards the peptide degradation, and most importantly elevate the circulation time in biological environments. Despite of these, PEG is a compound which possesses many advantageous properties; could be listed as high hydrophilicity, low viscosity, non-immunogenicity and low cytotoxicity[46] etc. In this research work peptide conjugation are strongly influenced by the NHS ester mediated PEGylation as the activated NHS ester effectively reacts with free amino group of the peptide under mild conditions thus form a stable bond formation. As mentioned in one of the articles [47] generally it is appropriate to use monomethoxylated form of PEG in protein conjugation as its mono functionality yield cleaner chemistry. The incorporation of PEG linker to a biomolecule could highly reduce the steric hindrance between the biomolecule and the functional moieties; in this thesis work the steric hindrance between the FNA-S-ACooP and the carborane moiety and enhances the molecular flexibility during the conjugation reactions. The specific properties of PEG has contributed to this flexibility such as mass, number of linking chains, the molecular site of PEG attachment [44].

In contrast, it is significantly important to optimise the PEGylation strategies in order to mitigate the PEGylation related problems such as excessive PEGylation, stoichiometry of reagents, pH, solvent composition, purification conditions and optimised analytical methods such as LC-MS, MALDI/TOF etc.

2.12 1,3 dipolar cycloaddition reaction in click chemistry

Click chemistry has become an important synthetic method in bioconjugation and medicinal chemistry. The most popular reaction among various click reactions is copper catalysed azide alkyne cycloaddition (CuAAC) conceptualized by Rolf Huisgen in 1960 and it was widely used in organic material and biological chemistry[48]. The potential of this reaction is immensely high as it involves alkyne and azide compounds; has capacity of integrating with wide range of substituents[49]. CuAAC reactions based on 1,3 dipolar cycloadditions resulting the formation of stable 1,2,3 triazole linkages as shown in figure 5[50].A significant property with this reaction mechanism is the ability of use variety of solvents with numerous solvent conditions[50]. For example, with non-coordinating solvents, such as toluene and chloroform, with weakly

coordinating solvents as pyridine and dioxane, with polar solvents such as ACN, DMF, DMSO and in this thesis work $CuSO_4$ and sodium ascorbate. Based on these properties it is preferentially selective in peptide chemistry and target biomolecule conjugation approaches. A notable advantage of this click chemistry is its bioorthogonal nature[49] in context of react selectively without interfering with naturally existing biological functionalities. That is the reason for selecting CuAAC as appropriated for PEGylate conjugates where selective and controlled functionalised conditions are applied. The outcome of the reaction is the triazole linkage and it indicates high chemical metabolic stability which is beneficial towards the biological relevant conjugates and radiopharmaceutical candidates. In contrast the PEG spacer act as a molecular linker or flexible bridge in-between peptide and the carborane cluster which improves the molecular flexibility and accessibility of the target group during the conjugation or coupling. However, it is required to optimize the reaction conditions such as catalyst concentration reagent stoichiometry pH and the reaction time in order to facilitates and improve the conjugation efficiency.

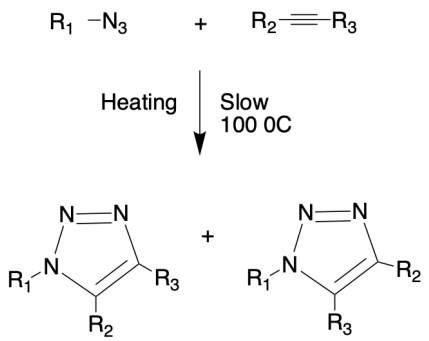

Figure 7: *Formation of stable 1,2,3 triazole linkages during 1,3 dipolar cycloadditions*

3 Study aims

The key goal of this study was to develop a novel 18F labelled carborane- peptide conjugate as a potential boron carrier molecule for BNCT. It is a highly selective cancer treatment modality that relies on the effective accumulation of boron-10 within tumour cells, subsequently neutron irradiation to induced localised cytotoxic effects. Hence, the success of BNCT is greatly influenced by on the design of suitable boron carrier. The boron carrier molecules selectively target tumour tissues while maintaining healthy or favourable pharmacokinetic properties. In this research, a peptide-based targeting approach was incorporated using the radiolabelled peptide [^{18}F]FNA-S-ACooP which provides a platform for boron delivery. This study aimed at the conjugation of a carborane cluster as a boron rich moiety to the peptide structure in order to elevate the boron accumulation with the target cells. In this study, two different strategies were investigated as follows.

1. **1.** Direct carborane-peptide conjugation
2. **2.** Alternative approach to the conjugation rection via PEGylated linker (polyethylene glycol PEG)

The direct conjugation approach was intended to achieve a straightforward coupling reaction between the carborane and the peptide. Implementation of PEG linker strategy was exploded, in order to improve conjugation efficiency, reduce steric constrains and optimize the overall physicochemical properties of the resulting conjugate. Along with this PEGylation was expected to improve solubility and presumably influence the biological behaviour of the system including stability and distribution. By comparing these two strategies, this research aimed to identify an effective approach for synthesising stable and functional carborane-peptide conjugates.

Collectively, this research aimed to contribute to the development of advanced boron delivery system by integrating radiochemistry and peptide-based targeting. The successful synthesis and characterisation of ^{18}F-labelled carborane peptide conjugates have the potential to provide foundation for further studies about BNCT, significantly in the design of theranostic agents that combine diagnostic imaging and targeted therapy.

4 Materials and methods

4.1 Chemicals and equipment

Chemicals used for HRMS and NMR analysis were all analytical graded. Methanol (Honeywell, Seelze, Germany) Methanol hyper grade for LC-MS (Merck, Darmstadt, Germany), Acetonitrile (Honeywell, Seelze, Germany), N,N-Dimethylformamide (Sigma Aldrich, Saint Louis, USA), Formic acid (Sigma Aldrich, Saint Louis, USA), trifluoroactetic acid (Sigma Aldrich, Saint Louis, USA) were used as received. (Fluoronicotinic acid 4- nitrophenyl ester was made in large volume inhouse. For NMR analysis deuterated DMSO (Eurisotop). ACooP peptide-AGLSCGLGVA (C-terminus: NH_2) (United peptide) FPy-CooP in house made and used as a reference. Dimethylsulphoxide D6 (Eurisotop). For the coupling reaction hexafluorophospate azabenzotriazole tetramethyl uranium (HATU)(TCI), N, N-diisopropylethylamine (DIPEA) (Sigma Aldrich, Saint Louis, USA), m-carborane-1-carboxilic acid from university of Helsinki and used as received, -(2,5-Dioxopyrrolidin-1-yl)-1,1,3,3-tetramethylisouronuim tetrafluoroborate (TSTU)(BLDpharm, Reinbeck, Germany). Sodium borate (Sigma Aldridge, MO, USA), sodium hydroxide (Sigma Aldridge, MO, USA) also used as received. Azido PEG_2-NHS-ester (Broad pharm, San Diego, USA), propargyl-PEG_3-amine (Broad pharm, San Diego, USA), (Sigma Aldrich, Saint Louis, USA). Deionised water was from Milli-Q Ultrapure water purification system.

Sep-pak plus light C18 cartridge (WAT023501). For HRMS filter (Choice 25mm, 0.22 μm RC (CH22225-RC) from Thermo scientific). Jupiter 5 μl C-18 300 Å 150 x 4.6 mm column, Aeris^{TM} 5μ PEPTIDE column, Jupiter^{R} 4 m Proteo 90 Å LC column 250 x 10 m, analytical weight scale (100A-300M, Precisa),for weighing of eppendorf tubes by Mettler Toledo xs 105 (dural range), BUCHI rotovapor R-100 along with BUCHI heating bath B-100 (BÜCHI labortechnik AG, Falawi, Switzerland). Vaccume concentrator Heto-CT-60E vaccume concentrator connected to a vaccubrand RC 5 chemistry hybrid vacuum pump (Vacuubrand GmbH+ Co, Wertheim, Germany)

4.2 Analytical techniques

4.2.1 High performance liquid chromatography (HPLC)

For this thesis work, LaChrome Elite HPLC system (Hitachi, Ltd, Tokyo, Japan) was used; along with L-2130 pump and L-2400 UV detector, operated through EZchrome Elite software. This HPLC was used for the purification of non-radioactive products. Analytical and isolation HPLC analyses were performed on a Shimadzu HPLC system (Kyoto, Japan)[51] featuring an LC-40 pump and SPD-40 UV-Vis detector. The system operation was controlled through the LabSolutions software. For both the systems NaI(TI) scintillation detector was coupled to the UV in order to detect the radioactivity. There was a slight time delay between the UV and radiation detectors due to their position difference. Mobile phase flow rate, internal diameter of the tubing distance between the detectors are contribute for this delay.

For this thesis work the reverse phase HPLC was widely used. In reverse phase chromatography there is a high polar mobile phase and a non-polar solid phase, and the non-polar solid phase could be octadecyl or octa functionalised silica gel[52]. Generally, in the reverse phase HPLC (RP-HPLC) the non-polar compounds are eluted after the polar compounds which means compounds are eluted in reverse polarity order. By increasing the percentage of acetonitrile in water can be used as the mobile phase mixture when performing RP-HPLC. In this thesis work isolation and purification of non-radioactive products and the conjugated compounds were performed with Shimadzu HPLC system set up with the reverse phase HPLC columns Jupiter 5 μl C-18 300 Å 150 x 4.6 mm column, Aeris^{TM} 5μ PEPTIDE column, Jupiter^{R} 4 m Proteo 90 Å LC column 250 x 10 m with a UV detector, radioactivity detector as mentioned above.

HPLC is a high performing and effective chromatographic technique for analysing and purifying analyes in a mixture. As the main structural components of the sytem are solvent pump , sample injecter, column, detection system, and the data acquisition system. The solvent delivery system delivers the solvent at high pressure through the solid phase incorporated within the column. Multiple solid phases are available for analytical and semi preparative applications each demonstrating different properties such as particle size, column length and diameter. The columns are manufactured from stainless steel and packed with micrometre size solid phase particles to achieve improved resolution and efficient separation. The samples injector into the column could be operated either manually or automatically[53].The compounds are separated as they pass through the column and followed by reaching the detector where they can be identify by detecting according to the characteristics of the analyte. Ultraviolet/visible (UV/Vis), photodiode array, fluorescence, and conductivity detectors are the most common detectors which includes in HPLC system. There could be contained radiation detectors as additionally. The time period required for the analyte to pass through the column and reach the detector known as the retention time of the particular analyte [54]

Table 1: *HPLC columns and methods employed during the analysis*

Method	Column	Compound analysed	Eluent conditions	Flowrate(mL/min)	Wavelength λ (nm)
(i) Analytical	C-18 Jupiter® 5 μm 300Å 150 x 4.6 mm	FNA-S-ACooP	**A:** 0.1% TFA in water **B:** 0.1% TFA in ACN	1	220 254
(ii) Analytical	C-18 Aeris™ PEPTIDE XB 5 μm 100 Å 150 x 4.6 mm	Carborane-N-FNA-S-ACooP	**A:** 0.1% TFA in water **B:** 0.1% TFA in ACN	1	220 254
(iii) Semi preparative	C-18 Jupiter® 4μm Proteo 90Å 250 x 10 mm	FNA-S-ACooP	**A:** 0.1% TFA in water **B:** 0.1% TFA in HCOOH	5	220 254
(iv) Semi preparative	C-18 Jupiter® 4μm Proteo 90Å 250 x 10 mm	FNA-S-ACooP-N-PEG_2-N_3	**A:** 0.1% TFA in water **B:** 0.1% TFA in HCOOH	5	220 254

4.2.2 Nuclear magnetic resonance (NMR)

In this research NMR spectra were obtained on a 600 MHz Bruker Avance III spectrometer (Bruker, Billerica, MA, USA). The solvent used for NMR samples was *d*6-DMSO (Eurostop, France) and it was a deuterated solvent. The operation frequencies for ^{1}H and ^{12}C were 600 MHz and 125.75 MHz respectively. For the conformation of the structure 1D and 2D both methods are performed. Chemical shifts(δ) are recorded in parts per million (ppm) and it was calculated with respect to the residual peak of the deuterated solvents[55]. Spectral splitting patterns are abbreviated as singlets (s), doublets (d), triplets(t), quartet(q), multiplet (m), and broad singlets (br s). Coupling constants are marked as *j* values are measured with Hertz (Hz). The two-dimensional (2D) NMR performed including Total Correlation Spectrometry (TOCSY) and the obtained data was possessed by using Bruker topspin software.

NMR spectroscopy is one of the major important analytical modalities, specifically to use the structural characterisation of chemical compounds. NMR provides detailed information about the molecular structure based on the magnetic characteristics of nuclei with an odd mass number that shows spin angular momentum (for ex: ^{1}H, ^{19}F, ^{13}C,^{11}B, ^{31}P). Further it provides the detailed information about chemical environment and connectivity of atoms within a compound. In this technique when the compound subjected to and external magnetic field those nuclei absorb the electromagnetic radiations at characteristic resonance frequencies. Therefore, this technique is broadly used for confirming the identity and purity of synthesized compounds.

4.2.3 High resolution Mass spectrometer (HRMS)

In this thesis work the mass analysis and chromatographic characterisation of the synthesised compounds were performed by using Acquity premier ultra performance liquid chromatography (Waters corporation, Milford, MA, USA) coupled with time of flight (TOF) mass spectrometer along with electrospray ionisation (ESI). Data acquisition mode was positive ionisation mode (ESI+) using MSe acquisition mode. Mass spectra were obtained over m/z range of 400-7000 with the cone voltage of 30V.

Chromatographic separations were carried out using an Aquicty premier UPLC system coupled with a quaternary solvent manager, sample manager FTN, column manager and PDA eλ detector. For the purpose of compound characterisation and the purity assessment, UV absorbance and mass spectral data were simultaneously collected. Molecular ions corresponding to the protonated species (forex:$[M+H]^{-}$and multiplied charged peptide ions were detected and employed for molecular weight confirmation of the synthesised products.

Chromatographic acquisition, mass spectral analysis, peak integration, retention time determination, acquire mass processing and the instrumental control was executed by Waters empower and water connect software platforms. By analysing acquired UPLC- MS data it is possible to come to conclusions, monitor the reaction progress, evaluate purification efficiency, and to confirm the successful synthesis of the product compound.

4.3 Synthesis, purification and characterisation of target analytes FNA-S-ACooP, of Carborane N-FNA-S-ACooP, FNA-S-ACooP-N-PEG_2-N_3 and carborane-N-propargyl-PEG_3 conjugation

4.3.1 Synthesis and purification of FNA-S-ACooP

1.5 mL protein lobind Eppendorf tube was charged with ACooP peptide (5.00mg, 6.44μmol) and added 1006 μL water (Trace SELECT Honeywell). To another 1.5 mL protein lobind Eppendorf tube added fluoronicotinic acid (16.88 mg, 64.38 μmol) and added 1000 μL of acetonitrile (ACN). The following compounds were added to another 5 mL protein lobind Eppendorf tube: first, 132 μL of freshly prepared borate buffer (300mM, 8.6pH), then 400 μL of ACooP peptide and followed by adding another 132 μL of FNA and 600 μL of acetonitrile. After adding all reagents, it was observed a yellowish green colour solution. The mixture was vortexed and then left to react at room temperature for 10 minutes. Added 4 mL of water after 10 minutes of reaction time to make it more soluble for purification. The reaction mixture was filtered by using a solid phase extraction cartridge Sep-pack plus C-18 WAT 023501(Waters corporation, Milford, MA, USA) to remove all the unwanted ions, salt and other impurities in the reaction mixture before HPLC performed. The cartridge was preconditioned with 5mL of ACN and 20 mL of water. After the filtration of reaction mixture through the cartridge, the trapped product was eluted and collected by washing the cartridge with 5mL of ACN. Generally, this cartridge is used for trapping hydrophobic compounds in the reaction mixture, to concentrate the mixture before performs HPLC analysis. Further, these filters contain reverse phase C-18 silica materials as the column. An analytical HPLC (Shimadzu) system was used to identify the retention time of the targeted analyte FNA-S-ACooP. The analytical HPLC analysis was performed by employing Jupiter® reverse phase column (150 × 4.6 mm, 5 μm particle size, 300 Å pore size: (Phenomenex, Torrance, CA, USA). HPLC solution A and B were prepared initially with 0.1% of trifluoroacetic acid (TFA) in water and 0.1% of TFA in acetonitrile respectively. The flowrate of the column was operated at 1.00 mL/min with a reverse phase gradient elution. The HPLC elution gradients that was used are illustrated in table 1. The HPLC method was run with a total run time of 25 minutes. The detection wavelengths were 220 nm and 254 nm. First, the reference run was carried out with FPy-CooP (1mM,) the inhouse reference and 10 μL of sample was injected to determine the retention time with the provided column and the conditions applied. The retention time was recorded at 4.92 minutes. 10 μL aliquot of the reaction mixture then subjected to the HPLC run. The primary peak of the targeted product was observed at the retention time of 5.35 minutes. The HPLC analysis of both reference and the reaction mixture was repeated three time to ensure the consistency of the results. Subsequently, the reaction mixture subjected to the purifying with the same column and it was conducted as a batch purification. Upon completion of the batch purification the following step was drying the product fractions. The drying was performed with Heto-CT-60E vaccume concentrator connected to a vaccubrand RC 5 chemistry hybrid vacuum pump (Vacuubrand GmbH+ Co, Wertheim, Germany). A white solid product appeared after efficient drying of the analyte samples in the centrifuge. Accurate mass measurements were recorded using a XS105 dural range analytical balance (Mettler Toledo, Greifensee, Switzerland) and the balance provided the readability of ± 0.01 mg for

low mass measurements. FNA-S-ACooP was afforded in 62.3% yield (1.8 mg, 1.9 μmol). Measured mass of the target products then subjected to HRMS and NMR analysis.

During the next phase of the procedure, purification of the target analyte FNA-S-ACooP was conducted with different HPLC solution. The analytical HPLC (LaChrome Elite) analysis was performed by employing Jupiter® Proteo C-18 reverse phase column (250 x 10 mm ,4μm particle size, 90Å pore size: Phenominex, Torrance, CA, USA). HPLC solution A and B were prepared with 0.1% of formic acid (HCOOH) in water and 0.1% of HCOOH in acetonitrile respectively. The HPLC elution gradients used for this analysis illustrated in table 2. The flowrate of the column was operated at 1.00 mL/min. the detection wave lengths were 220 nm and 254nm. The HPLC method was run with a total run time of 25 minutes. First, the reference run was carried out with FPy-CooP (1mM) the inhouse reference and 10 μL of sample was injected to determine the retention time with the provided column and the conditions applied. The retention time was recorded at 4.92 minutes. Subsequently the 10 μL of the reaction mixture was subjected to HPLC by providing the same elution gradient as for the reference and the retention time was recorded at 4.94 minuets. The product identity was further confirmed by performing a co-injection analysis with 1 μL of in house refence FPy-CooP(1mM) standard with the reaction mixture in the same HPLC vial. An increase in the peak area at the same retention time was interpreted as evidence for the presence of the target compound FNA-S-ACooP. Following determination of retention time, the purification of the reaction mixture was carried out as a batch purification. Upon completion of the batch purification the following step was drying the product fractions. The drying was performed with Heto-CT-60E vacuum concentrator as mentioned in the previous purification process. A white solid product appeared after efficient drying of the analyte samples in the centrifuge. The product mass was measured using XS105 dural range analytical balance as similar with the previous purification and it was recorded as 0.7 mg. The product was then subjected to HRMS analysis.

Table 2: HPLC gradients for FNA-S-ACooP by purifying with 0.1% TFA in water and ACN

Time after injection	ACN (0.1% TFA)	Water (0.1% TFA)	Flow rate
0 min	25 %	75 %	1 mL/min
10 min	50 %	50 %	1 mL/min
12 min	80 %	20 %	1 mL/min
15 min	25 %	75 %	1 mL/min
20 min	25 %	75 %	1 mL/min

Table 3: HPLC gradients for FNA-S-AcooP by purifying with 0.1% HCOOH in water and ACN

Time after injection	ACN (0.1% TFA)	Water (0.1% TFA)	Flow rate
0 min	25 %	75 %	1 mL/min
10 min	50 %	50 %	1 mL/min
12 min	80 %	20 %	1 mL/min
15 min	25 %	75 %	1 mL/min
20 min	25 %	75 %	1 mL/min

4.3.2 Characterisation of FNA-S-ACooP

Characterisation of the target product has been carried out with HRMS analysis and the NMR analysis. FNA-S-ACooP was afforded in 62.3% yield (1.8 mg, 1.9 μmol). t_R = 2.07 ^{1}H NMR (500.06 MHz, DMSO-D_6) δ 8.76 (d, *J* = 8.8 Hz, 1H), 8.43 (t, *J* = 3.7, 2H), 8.26 (s, 1H), 8.22 (t, *J* =4.8 Hz, 2H), 8.1 (d, *J* = 7.5 Hz, 1H), 8.05 (d, *J* = 8.2 Hz, 1H), 7.99 (d, *J* = 7.7, 1H), 7.74 (d, *J* = 8.6 Hz, 1H), 7.38 (q, *J* = 3.65 Hz, 3H), 7.19 (s, 1H), 6.95 (s,1H), 4.56 (t, *J* = 6.7 Hz, 2 H), 4.38 (q, *J* = 7.6 Hz, 3H), 4.28 (quint, *J* = 6.3 Hz, 4H), 4.12 (sext, *J* = 7.6 Hz, 4H), 3.8 (s,1H), 3.74 (q, *J* = 5.8 Hz, 2H), 2.61 (t, *J* = 1.7 Hz, 1H), 2.38 (t, *J* = 1.7 Hz, 2H), 1.97 (sext, *J* = 6.7 Hz, 3H), 1.9(s, 1H), 1.58 (quint, *J* = 7.5 Hz, 3H), 1.47 (q, *J* = 4.3 Hz, 2H), 1.44 (t, *J* = 6.5 Hz, 1H), 1.21 (q, *J* = 6.7 Hz, 2H), 0.86 (t, *J* = 7.2 Hz, 2H), 0.83 (quint, *J* = 2.6 Hz, 2H), 0.79 (s,1H)ppm. To support the characterisation, it was performed a TOCSY analysis as well.

HRMS (ESI) m/z: $[M + H]^+$ calculated for $C_{41}H_{65}FN_{12}O_{12}S^+$ 969.45612; found 969.45602 (Δ = 4.8 ppm) minor adduct peaks corresponding to $[M + Na]^+$ observed at m/z 992.45064 and this was observed with the FNA-S-ACooP purified with TFA. When the target analyte purified with HCOOH; HRMS (ESI) m/z: $[M + H]^+$ calculated for $C_{41}H_{65}FN_{12}O_{12}S^+$ 969.45612; found 969.46361 (Δ = 0.8 ppm) minor adduct peaks corresponding to $[M + Na]^+$ observed at m/z 991.44418

4.3.3 Synthesis and purification of Carborane N-FNA-S-ACooP

Four 1.5 mL protein lobind Eppendorf tubes were charged with the following compounds and prepared stock solutions by dissolving them in DMF; DIPEA (19.39 mg, 150 μmol) was dissolved in 473 μL of DMF to prepare 316.9mM stock solution, HATU (29.7 mg, 78.1 μmol) was dissolved in 500 μL to prepare 156.2 mM stock solution , FNA-S-ACooP (1.64 mg, 1.7 μmol) was dissolved in 330 μL of DMF to prepare 5.1 mM stock

solution and M-carborane carboxylic acid (15.6 mg, 82.87 μmol) was dissolved in 500 μL of DMF to prepare 165.7 mM stock solution.

For the coupling reaction another 1.5 mL protein lobind Eppendorf tube was loaded with the following compounds; 111 μL of FNA-S-ACooP from the stock solution combined with 3 μL of DIPEA from the stock solution. 3 μL of HATU from the stock solution and 3 μL of M-carborane carboxylic acid from the stock solution combined to another 1.5 mL protein lobind Eppendorf tube. The reaction mixture was formed by adding FNA-S-ACooP and DIPEA solution dropwise (20 μL each drop) to the M-carborane carboxylic acid and HATU solution. Upon the complete addition the reaction mixture was gently agitated and allowed to react for 25 minutes at room temperature. Prior to further analysis, the reaction mixture was stored at -20 ^{0}C in the freezer. FNA-S-ACooP was afforded in 73.0 % yield (0.38 mg, 0.34 μmol). Measured mass of the target products then subjected to HPLC and HRMS analysis.

4.3.4 Characterisation of carborane N-FNA-S-ACooP

To determine the retention time of the target product carborane N-FNA-S-ACooP HPLC analysis was carried out. The reverse phase analytical HPLC (Shimadzu) analysis was performed by employing Aeris^{TM} PEPTIDE XB-C-18 column (5 μm particle size, 100 Å pore size,150 x 4.6 mm; Phenomenex, Torrance, CA, USA). HPLC solution A and B were prepared initially with 0.1% of trifluoroacetic acid (TFA) in water and 0.1% of TFA in acetonitrile respectively. The flowrate of the column was operated at 1.00 mL/min with reverse phase gradient elution. The HPLC elution gradients that was used illustrated in table 3. The HPLC method was run with a total run time of 25 minutes. The detection wavelengths were 220 nm and 254 nm. The reaction mixture was analysed 25 minutes after mixing each compound of the reaction. 10 μL aliquot of the reaction mixture subjected to HPLC analysis and the chromatogram showed a prominent peak at t_R = 23.67 minutes. In oder to monitor the progress of the reaction another HPLC analysis was performed in another 25 minutes (total reaction time of 50 minutes) and evaluate the increase in product formation. Separate HPLC runs were performed with the starting materials taking 10 μL of samples from the stock solutions of M-carborane carboxylic acid and FNA-S-ACooP in order to determine their individual retention times under the given conditions. The retention time was observed at t_R = 15.8 minutes with FNA-S-ACooP and it was recorded as t_R = 27.9 minutes for of M-carborane carboxylic acid.

Table 4: HPLC gradients of carborane N-FNA-S-ACooP by purifying with 0.1% TFA in water and ACN

Time after injection	ACN (0.1% TFA)	Water (0.1% TFA)	Flow rate
0 min	30%	70 %	1 mL/min
10 min	65%	35 %	1 mL/min
12 min	65%	35 %	1 mL/min
15 min	30 %	70 %	1 mL/min
20 min	30 %	70 %	1 mL/min

The target analyte was then subjected to HRMS analysis. HRMS analysis was performed under positive electrospray ionisation mode (ESI) using high mass acquisition as the method parameter. HRMS (ESI) m/z: $[M+H]^+$ calculated for $C_{44}H_{75}B_{10}FN_{12}O_{13}S^+$ 1141.65211; major peaks were observed at t_R = 3.4 minutes m/z 433.29764, m/z 587.40696, m/z 776.22760 and t_R = 3.2 minutes m/z 458.34875, m/z 502. 37709, m/z 644.39670, m/z 732.43497.

4.3.5 Conjugation of Azido-PEG_2-NHS-Ester and FNA-S-ACooP to synthesis FNA-S-ACooP-N-PEG_2-N_3

An empty protein lobind Eppendorf tube of 1.5 mL charged with azido PEG_2-NHS-ester (2.4 mg, 7.99 μmol) and it was dissolved in 100 μL of DMF to prepare 79.9 mM of stock solution. To another 1.5 mL empty protein lobind Eppendorf tube added FNA-S-ACooP (0.7 mg, 0.07μmol) and it was dissolved in 140 μL of DMF to prepare 0.52 mM of stock solution. 174 mL of borate buffer (300mM, 8.6pH) was collected to another 1.5 mL protein lobind Eppendorf. Upon completion of preparation of stock solutions, azido PEG_2-NHS-ester was added to the Eppendorf tube which already contained borate buffer. Following, added 50 μL of FNA-S-ACooP to the reaction mixture and vortex well.

5 μL of freshly prepared reaction mixture was immediately subjected to the HPLC analysis. The reverse phase preparative HPLC (Shimadzu) analysis was performed by employing Jupiter® Proteo C-12 reverse phase column (250 x 10 mm ,4μm particle size, 90Å pore size: Phenominex, Torrance, CA, USA). HPLC solution A and B were prepared initially with 0.1% of trifluoroacetic acid (TFA) in water and 0.1% of TFA in ACN respectively. The flowrate of the column was operated at 5.00 mL/min with reverse phase gradient elution. The HPLC method was run with a total run time of 20 minutes. The detection wavelengths were 220 nm and 254 nm The HPLC elution gradients that was used illustrated in table 4. Major peaks were observed at the following retention times t_R = 3.038 minutes, t_R = 5.006 minutes t_R = 5.566 minutes. Allowed the reaction mixture to react under the room temperature for 3 hours. After 3 hours, peak intensity was observed any increase during the reaction by performing HPLC analysis with 10 μL of the reaction mixture. The fractions from retention times t_R = 3.038 minutes, t_R = 5.006 minutes t_R = 5.566 minutes collected and

dried overnight with Heto-CT-60E vacuum concentrator. The measured weights of the samples are 0.72 mg, 0.42 mg, 0.97 mg respectively. The purified samples then subjected to HRMS analysis and revealed the components correspond with the retention times, which were collected during HPLC analysis. It was recorded as t_R = 5.006 minutes as FNA-S-ACooP (1 mg/mL) retention time t_R = 3.038 minutes of Azido PEG_2-NHS-ester (1 mg/mL) and a t_R =5.566 as FNA-S-ACooP-N-PEG_2-N_3 (1 mg/mL) in HRMS analysis.

During the next phase of the procedure, purification of the target analyte azido FNA-S-ACooP-N-PEG_2-N_3 was performed with different HPLC solution. The reverse phase preparative HPLC (Shimadzu) analysis was performed by employing Jupiter® Proteo C-12 reverse phase column (250 x 10 mm ,4μm particle size, 90Å pore size: Phenominex, Torrance, CA, USA). HPLC solution A and B were prepared with 0.1% of formic acid (HCOOH) in water and 0.1% of HCOOH in acetonitrile respectively. The HPLC elution gradients used for this analysis illustrated in table 5. The flowrate of the column was operated at 5.00 mL/min and the detection wave lengths were 220 nm and 254nm. The HPLC method was run with a total run time of 20 minutes. Under the same HPLC conditions as with TFA, the HPLC analysis with HCOOH also indicated the same chromatographic peak patterns correspondence with retention time interested, but the retention times were slightly shifted than comparative to the previous chromatogram. Hence, it was recorded t_R = 3.228 minutes, t_R = 4.576 minutes t_R = 4.753 minutes as retention times corresponded to the previous chromatogram. The fractions from the target compound were collected as a HPLC batch purification and subjected to overnight drying with Heto-CT-60E vacuum concentrator. The weight of the samples corresponded with the retention times were 0.52 mg, 0.7 mg, 0.42 mg respectively. The purified samples then subjected to HRMS analysis and revealed the components correspond with the retention times, which were collected during HPLC analysis. It was confirmed that t_R = 4.576 minutes as FNA-S-ACooP (1 mg/mL) retention time t_R = 3.228 minutes of Azido PEG_2-NHS-ester (1 mg/mL) and a t_R = 4.753 as FNA-S-ACooP-N-PEG_2-N_3 (1 mg/mL) in HRMS analysis. The synthesis was repeated two time to achieve sufficient weight of the target analyte FNA-S-ACooP-N-PEG_2-N_3 (0.64 mg) collectively. The sample then subjected to NMR analysis.

Table 5: HPLC gradients of FNA-S-ACooP-N-PEG_2-N_3 by purifying with 0.1% TFA in water and ACN

Time after injection	CAN (0.1% TFA)	Water (0.1% TFA)	Flow rate
0 min	25 %	75 %	5 mL/min
10 min	50 %	50 %	5 mL/min
12 min	80 %	20 %	5 mL/min
15 min	25 %	75 %	5 mL/min
20 min	25 %	75 %	5 mL/min

Table 6: HPLC gradients of FNA-S-ACooP-N-PEG$_2$-N$_3$ by purifying with 0.1% HCOOH in water and ACN

Time after injection	ACN (0.1% TFA)	Water (0.1% TFA)	Flow rate
0 min	20 %	80 %	5 mL/min
10 min	50 %	50 %	5 mL/min
12 min	50 %	50 %	5 mL/min
15 min	50 %	50 %	5 mL/min
20 min	80 %	20 %	5 mL/min

4.3.6 Characterisation of FNA-S-ACooP-N-PEG$_2$-N$_3$

Characterisation of the target FNA-S-ACooP-N-PEG$_2$-N$_3$ (purified with TFA) product has been carried out with HRMS and NMR analysis. The fractions collected from HPLC with the following retention times t_R = 3.228 minutes, t_R = 4.576 minutes t_R = 4.753 minutes were subjected to HRMS analysis. HRMS analysis was performed under positive electrospray ionisation mode (ESI) using low mass acquisition as the method parameter. Prior to analysis, the molecular structures of the target compounds (FNA-S-ACooP, azido PEG$_2$-NHS-ester, FNA-S-ACooP-N-PEG$_2$-N$_3$) were imported to the HRMS software UNIFI to generate the exact molecular masses and fragmentation patterns supported compound identification. The acquired spectra were compared with the theoretical data; the main peak intensities and fragmentation patterns along with the retention times to identify the presence of the target compound. Detection was based on the agreements between the observed chromatographic peaks corresponding m/z values, and fragmentation pattens. The identified compounds were further visualized and quantified (with detector count and detector response) by the software through the corresponding molecular structure assignment. The purified fractions were then subjected to NMR analysis. As the purification of HPLC with different solvent system (0.1% of HCOOH in water and 0.1% of HCOOH in acetonitrile) the experiment was repeated and with samples, it was performed both HRMS and NMR analysis. FNA-S-ACooP-N-PEG$_2$-N$_3$ was afforded in 56.8% yield (0.64 mg, 0.56 μmol). t_R = 2.07 ^{1}H NMR (500.06 MHz, DMSO-D$_6$) δ 10.39 (s, 1 H), 8.25 (d, *j* = 4.4 Hz, 1H), 4.88 (s, 2H), 4.64 (s,2H), 4.03(d, , *j* = 4.2 Hz,1H), 4.02 (d, , *j* = 4.2Hz, 1H), 3.89 (q, , *j* = 5.9 Hz,2H), 3.66 (q, , *j* = 6.4 Hz 2H), 3.6(sext, , *j* = 2.3 Hz, 2H), 3.54 (d, , *j* = 2.1 Hz, 2H), 3.53 (s,1H), 2.89 (s, 1H), 2.67 (t, *j* = 6.1 Hz, 2H) 2.61 (quint, , *j* = 1.8 Hz, 6H), 2.59 (s,1H), 2.42 (t, , *j* = 7.1 Hz, 2H), 2.36 (t, *j* = 6.3 Hz, 6H), 2.27(t, , *j* = 14.8 Hz, 6H), 2.18 (q, , *j* = 4.7 Hz, 1H), 2.1 (s, 1H), 2.17 (s, 1H), 1.90 (S, 1H), 1.50(t, , *j* = 7.1 Hz, 4H), 0.85 (t, , *j* = 6.9 Hz, 6H) ppm. To support the characterisation of the compound it was performed a HSQC analysis as well.

HRMS (ESI) theoretical monoisotopic singly charged mass $[M + H]^+$ for $C_{48}H_{76}FN_{15}O_{15}S^+$ m/z 1153.54312; and observed at m/z 1127.52183 (Δ = -9.5 ppm) theoretical doubly charged mass $[M + 2H]^{2+}$ m/z 576.77160 and observed at m/z 571.41221 when purified the analyte with TFA. When the target analyte purified with HCOOH; HRMS (ESI) theoretical monoisotopic singly charged mass m/z: $[M + H]^+$ for $C_{48}H_{76}FN_{15}O_{15}S^+$ 1153.54312; found m/z 1154.55163 (Δ = 0.8 ppm) minor adduct peaks corresponding to $[M + Na]^+$ observed at m/z 1176.53311.

4.3.7 Synthesis carborane-N-propargyl-PEG$_3$ conjugation

To a 1.5 mL protein lobind Eppendorf tube added m-carborane-carboxylic acid (2.82 mg, 15 μmol). Added tetramethylisouronium tetrafluoroborate (TSTU) (5.97 mg, 15.8 μmol). Mixed the compounds and added DMF (30 μL) into the reaction mixture. Subsequently, was added DIPEA (5.23 μL) as the base addition to the reaction mixture. Stirred the reaction mixture for 5-15 minutes by using a magnetic stir bar on a magnetic stirrer at room temperature. Following this, added propargyl-PEG$_3$-amine (2.8 μL, 15 μmol) and added DMF (20 μL) to sum up the volume 50 μL. The reaction mixture further stirred for 1-3 hours.

4.3.8 Characterisation of carborane-N-propargyl-PEG$_3$ conjugation

10 μL of propargyl-PEG$_3$-amine (1mM) sample was subjected to HPLC analysis to determine the retention time. 10 μL of m-carborane-carboxylic acid (1mM) also performed with HPLC analysis to determine the retention time under the same HPLC conditions. The reverse phase analytical HPLC (Shimadzu) analysis was performed by employing Aeris^{TM} PEPTIDE XB-C-18 column (5 μm particle size, 100 Å pore size,150 x 4.6 mm; Phenomenex, Torrance, CA, USA). HPLC solution A and B were prepared initially with 0.1% of TFA in water and 0.1% of TFA in acetonitrile respectively. The flowrate of the column was operated at 1.5 mL/min with reverse phase gradient elution. The HPLC elution gradients that was used illustrated in table 6. The HPLC method was run with a total run time of 45 minutes. The detection wavelengths were 220 nm and 254 nm. The retention time recorded for propargyl-PEG$_3$-amine (1mM) was t_R = 7.7 minutes whereas the retention time for m-carborane-carboxylic acid (1mM) was t_R = 27.953 minutes under same HPLC conditions. The reaction mixture (10 μL) was then subjected to HPLC analysis and the retention time of the target analyte (carborane- propargyl-PEG3) was observed at t_R = 27.96 minutes. Purification of the reaction mixture carried out as a batch purification and followed by overnight drying with Heto-CT-60E vacuum concentrator. The carborane- propargyl-PEG3 was afforded 44.6% (1.32 mg, 3.69 μmol).). The sample then subjected to HRMS for preliminary analysis.

Prior to HRMS analysis, DIPEA was removed by performing a small, scaled liquid-liquid extraction followed by rotary evaporation. Added 20 mL of DMF into the reaction mixture and dissolved faster by vortex. Into a closed 50 ml scale separatory funnel, added the reaction mixture and 20 mL of water shook vigorously and collected the water phase out of the separatory funnel and repeated for six times and followed by the rotary

evaporation with BÜCHI rotavapor coupled with a vacuum pump V-100 and heating bath B-100 (BÜCHI labortechnik AG, Falawi, Switzerland). The temperature of the hot bath was set to 40 ^{0}C and the pressure was 643 mbar in the vacuum pump. The agitated weight of the analyte sample was 0.78 mg (2.18 μmol).

5 Results and Discussion

5.1 Synthesis of FNA-S-ACooP

FNA-S-A-CooP was synthesized successfully with an overall yield of 62.3% as illustrated in figure 8.

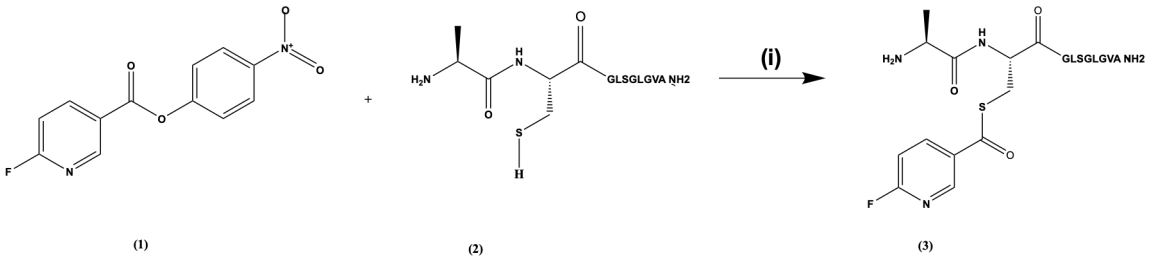

Figure 8: *Synthesis of FNA-S-A-CooP: FNA **(1)**; ACooP **(2)**; FNA-S-ACooP **(3)**; (i) borate buffer 90mM, pH 8.6, acetonitrile (70% by volume), 10 min, R.T*

The reaction between FNA **(1)** with ACooP **(2)** was performed using the activated prosthetic group fluoronicotinic acid derivative (FNA). The ACooP **(2)** served as the biomolecule targets $FABP_3$ which are abundantly available in the cancer cells. The reaction progressed through the acylation of the nucleophilic functional groups present in the peptide. Existing literature initially identified the conjugation products as FNA-S-ACooP **(3)** indicating N-acylation at the free amino terminus of the peptide. Despite this, subsequent structural characterisation showed that the major product formed under given reaction conditions was FNA-S-ACooP **(3)**, suggesting preferential S acylation at the thiol group of cysteine rather than N acylation at the amino terminus. The ACooP **(2)** contains both a free amino group and a free thiol group, therefore the chemo selectivity is highly dependent on the reaction and the purification conditions. The accessibility of the free amino terminus plays an important role in facilitating efficient N- acylation.

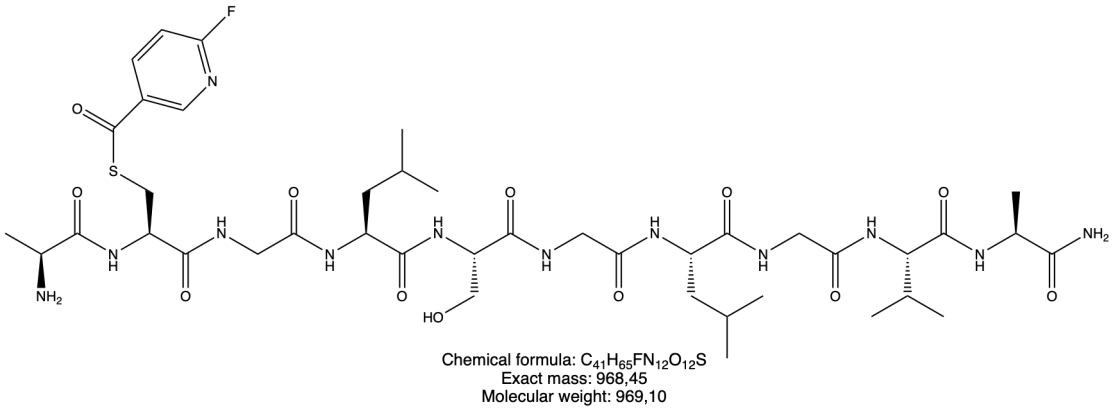

Figure 9: *Expanded molecular structure of FNA-S-A-CooP*

5.1.1 Characterisation of FNA-S-ACooP by HPLC analysis

During peptide purification using TFA the retention time of FNA-S-ACooP **(3)** was recorded at 4.98 minutes with the purified QC sample, and it was recorded as 4.94 minutes with the inhouse reference as shown in figure 10.

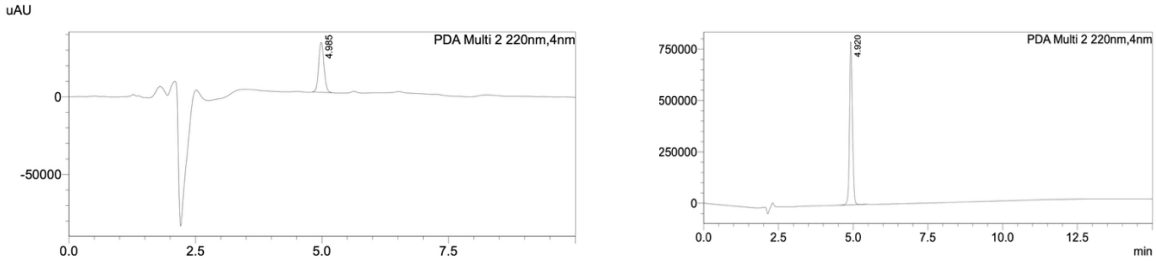

(1) ***(2)***

Figure 10: *Identification and quality control (QC) of purified FNA-S-ACooP* ***(3)*** *with TFA; HPLC chromatograms of;* ***(1)*** *retention time of FNA-S-ACooP (QC sample)* ***(2)*** *retention time of FNA-S-ACooP in-house reference under UV detection.*

When peptide purification carried out with TFA the free amino terminus exists predominantly in its protonated free amino salt form due to the strong acid condition as shown in figure 11. Protonation reduces the nucleophilicity of the amino group hence, decreasing its reactivity in the direction of conjugation with the activated FNA **(1)** prosthetic group. Subsequently, competing S acylation at the thiol group be promoted.

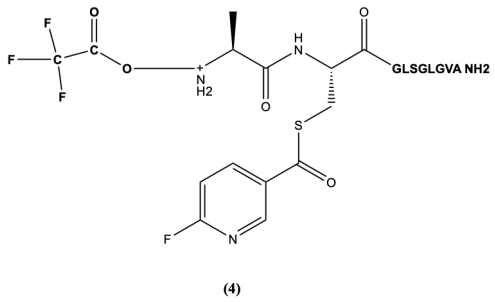

(4)

Figure 11: *Schematic representation of protonated N terminal ammonium trifluoroacetate salt of FNA-S-ACooP* ***(4)*** *formed during purification with TFA*

Purification using formic acid (HCOOH) provided improved conjugation efficiency in the subsequent reaction, which means the conjugation between FNA-S-AooP and Azido PEG_2-NHS ester. Comparative to TFA, HCOOH is a weaker acid, and it improve and enhance the recovery of peptide and providing better access to reactive free amino terminus. Although purification of FNA-S-ACooP **(3)** using HCOOH resulted in lower isolated yield 46% the subsequent conjugation product was identified more efficiently in the following

reaction step, compared to purified using TFA. During peptide purification using TFA the retention time of compound **(3)** was recorded at 6.052minutes with the purified QC sample, and it was recorded as 6.002 minutes with the inhouse reference as shown in figure 12. This observation determined maintaining an amino terminus in a less strongly protonated state improved the reactivity of the peptide conjugation.

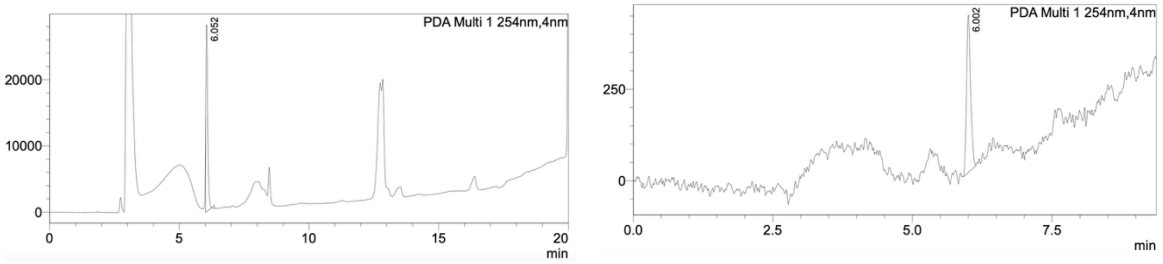

(1) ***(2)***

Figure 12: *Identification of the retention times of FNA-S-ACooP* ***(3)*** *with HCOOH; HPLC chromatograms of;* ***(1)*** *retention time of FNA-S-ACooP (QC sample)* ***(2)*** *retention time of FNA-S-ACooP in-house reference under UV detection.*

5.1.2 Characterisation of FNA-S-ACooP by HRMS analysis

Qualitative structural characterisation and compound identification of the analyte FNA-S-ACooP **(3)** was performed with HRMS. In this analysis it was focused the fragmentation patters, chromatographic peaks and comparison of expected m/z with exact mass. Figure 13 shows the results of HRMS analysis which revealed major chromatographic peak at retention time of t_R = 2.07 minutes. The theoretical monoisotopic mass of FNA-S-ACooP **(3)** was m/z 969.462 for the singly protonated molecular ion $[M + H]^+$.

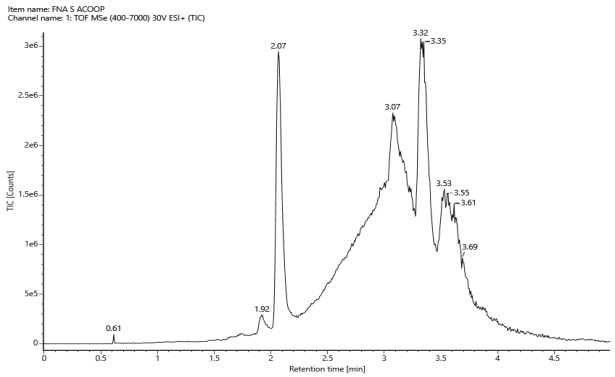

Figure 13: (1) *Total ion chromatogram (TIC) of FNA-S-ACooP purified with TFA*

The corresponding MS spectrum showed in figure6 (ii) in the appendices, a dominant peak at m/z 969. 45602 suggested with the expected molecular ion of FNA-S-ACooP **(3)**.

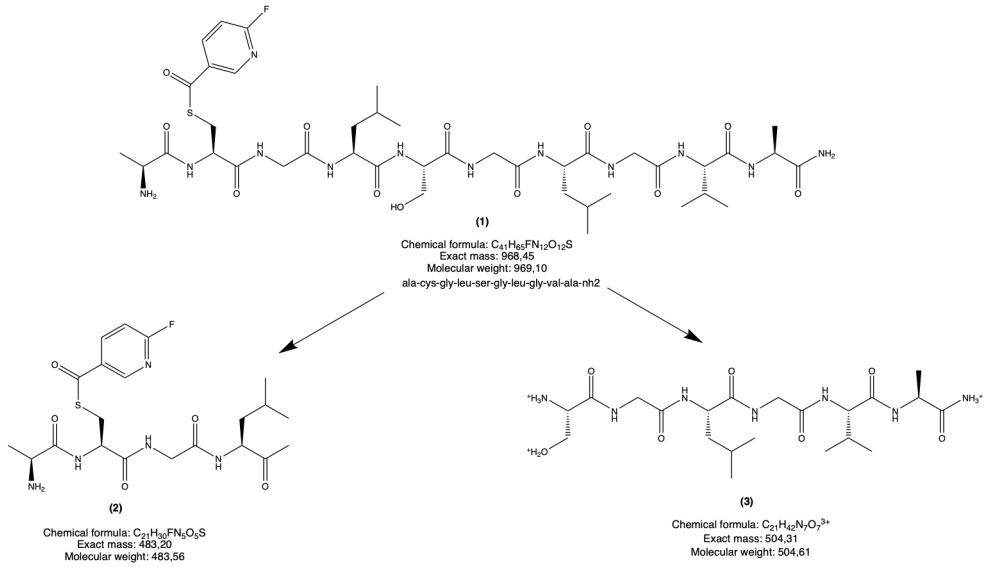

Figure 14: *Possible fragmentation patterns of FNA-S-ACooP* ***(1)****; corresponding fragmentations correlates with the peaks shown in figure 6 (****i****) in the appendix's m/z 483. 20 and* ***(3)*** *m/z 504.61*

Supplementary, additional lower intensity ions observed in the spectrum were attributed to isotope distributions, adduct species, and possible in source fragmentation products generated during electrospray ionisation (ESI). For example, the spectrum in figure 6 (ii) in the appendices shows possible fragmentation related ions includes m/z 483.20 and m/z 504. 31 are more likely fragment associated ions. The possible fragmentation pattens of FNA-S-A-CooP**(3)** are shown in figure 14. Fragment at m/z 991. 44932 and m/z 992. 45064 corresponding with an addiction of sodium ion $[M + Na]^+$.

HRMS analysis was conducted for the characterisation of HCOOH purified FNA-S-ACooP. The extracted ion chromatogram confirmed a major chromatographic peak at a retention time of t_R = 2.12 minutes. Corresponding to the expected protonated molecular ion of the analyte. The lower energy HRMS spectrum indicated a dominant ion at m/z 969.46361 with Δ = 1.4 ppm of mass error and which is in closely accordance with the theoretical $[M + H]^+$ ion of FNA-S-ACooP as shown in figure 15. The detector counts and the number of responses were also recorded as 92988 and 43911 respectively and the characteristic absorbance maximum wavelength at 214.1 nm as per the PDA analysis. Additional lower intensity ions showed at m/z 971.45556 and the peak correspondence with sodium adduct $[M + Na]^+$ showed at m/z 991.44418 were attributed to isotopic and adduct related species. The ions detected at lower m/z values likely originated from in ion source fragmentation products generated during ESI.

High energy MS analysis further supported the structural characterisation of the analyte through the observation of fragmentation related ions while maintaining the dominant parent ion at m/z 969.46394. The lower mass error suggested (1mDa) between the experimental and theoretical masses confirmed the accurate analysis of the detected analyte as shown in figure 17. Hence, HRMS results confirmed successful detection and characterisation of HCOOH- purified FNA-S-ACooP.

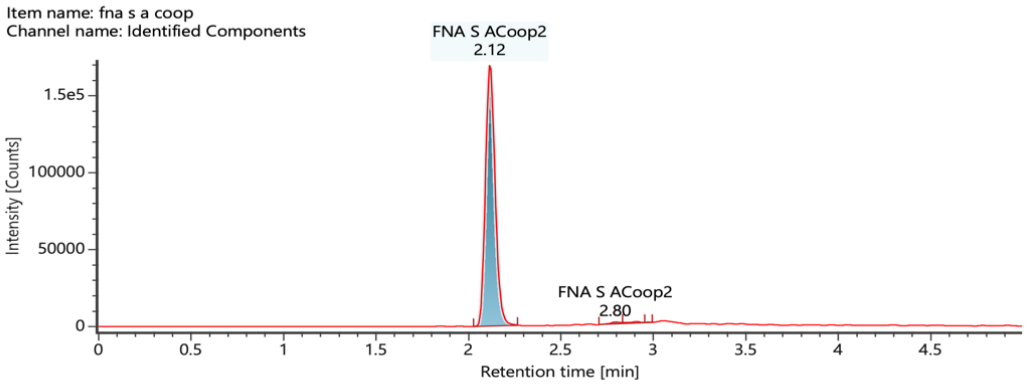

Figure 15: *Extracted chromatogram of HCOOH purified FNA-S-A-CooP indicating the major chromatographic peak at* t_R *= 2.12 minutes*

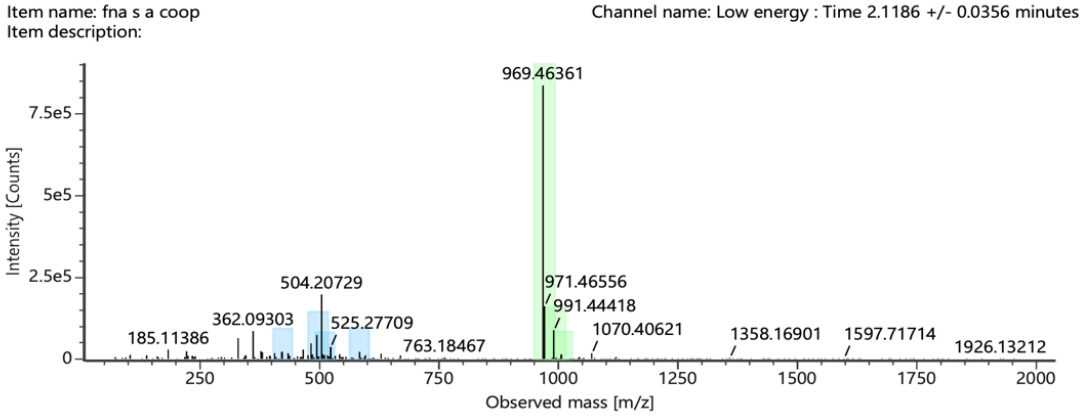

Figure 16: *HRMS spectrum of HCOOH purified FNA-S-A-CooP indicating the protonated molecular ion at m/z 969.46361*

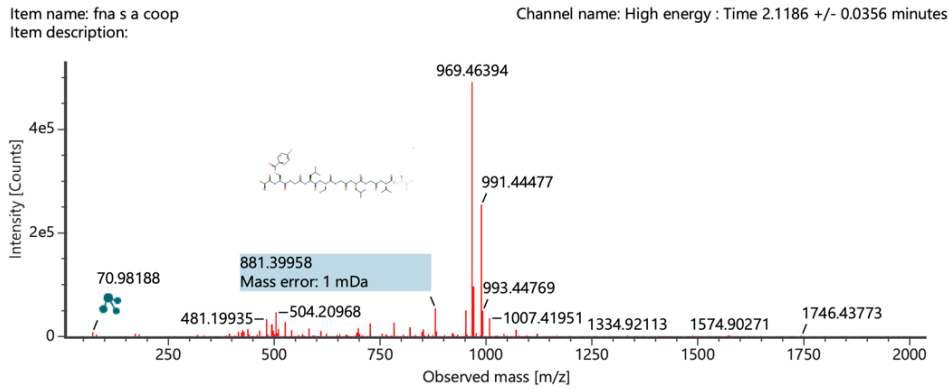

Figure 17: *High energy HRMS spectrum of HCOOH purified FNA-S-A-CooP fragmentation related ions and the dominant parent ion.*

5.1.3 Characterisation of FNA-S-ACooP by NMR analysis

Structural characterisation was successful with NMR analysis. It was able to identify the signals from the AcooP region (GLSGLGVA-NH_2/ ala, cys, gly, leu, ser,gly, leu,gly, val, ala-NH_2) with compared to the reference which illustrated in figure 2 in the appendices. The signals from the aromatic region (6.5 ppm-8.5 ppm) also significantly visible but some peaks supposed to be appeared in the region of 6 ppm to 7.5 ppm with comparative to the reference were not clearly visible in the spectrum. Some signals from the peptide region have been overlapped and resulted multiplicity in the spectrum significantly in the region of 0.5 ppm- 1.5 ppm. A broad peak related to residual water is observed 3.3 ppm -3.5 ppm which indicates that the residual moisture due to inadequate drying. There is a possibility of hindered signals in that particular area due to presence of broad residual water peak.

5.2 Synthesis of carborane-N- FNA-S-ACooP

Carborane-N-FNA-S-A-CooP**(3)** was synthesized as illustrated in figure 18.

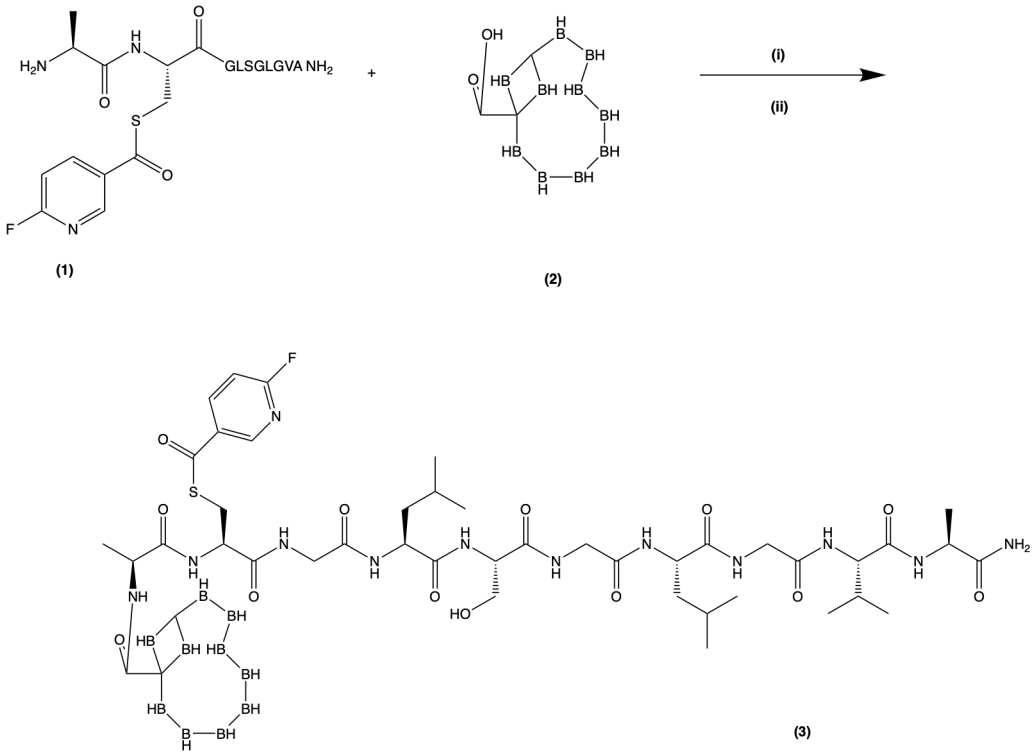

Figure 18: *represents the synthesis of Carborane-N-FNA-S-A-CooP* ***(3)****; starting materials are FNA-S-A-CooP* ***(1)*** *and m-carborane carboxylic acid* ***(2); (i)*** *DIPEA and* ***(ii)*** *HATU*

The synthesis of Carborane-N-FNA-S-A-CooP **(3)** was performed through an amide coupling reaction between the free N terminal amino group of FNA-S-A-CooP **(1)** and m-carborane carboxylic acid **(2).** In this reaction HATU **(i)** as the coupling reagent DIPEA **(ii)** as the base in DMF solvent to proceed the reaction. In terms of reaction mechanism, this involves nucleophilic acyl substitution in which the nucleophilic free amino group of FNA-S-A-CooP **(1)** attacks the activated carbonyl carbon of the m-carborane carboxylic acid

(2) derivative generated by HATU **(i)** activation resulting in amide bond formation following elimination of leaving group [56,57,58]. Compared to the other coupling reagents HATU is more effective as it enhance reactivity, depleted side productions and formation of racemization[59].

The incorporation of m-carborane moiety was a significant interest due to the unique chemical properties of carborane. Carboranes are boron rich polyhedral clusters. They possess high chemical stability, hydrophobicity and resistant towards metabolic degradation. The reason for attractive candidate for BNCT and radiopharmaceutical development is the high boron content of carborane. Conjugation of carborane moiety to the peptide base targeting vector FNA-S-A-CooP **(1)** was therefore expected to combine the targeting ability of the peptide with the favourable boron containing pharmacophore properties of the carborane scaffold. Efficient conjugation required accessibility of free and reactive amino terminus in the peptide FNA-S-A-CooP **(1).** Hence, purification conditions prior to the coupling reactions were very important because protonation or salt formation at the amino terminus could reduce nucleophilicity and negativity affect coupling efficiency.

5.2.1 Characterisation of carborane-N-FNA-S-ACooP by HPLC analysis

In the characterisation of carborane-N-FNA-S-ACooP, HPLC runs were performed with individual starting materials (FNA-S-ACooP and m-carborane carboxylic acid), during the reaction monitoring over the time and in the QC analysis of the product analyte (carborane-N-FNA-S-ACooP). The individual HPLC analysis of FNA-S-ACooP the chromatogram showed a major peak at the retention time of t_R = 10.826 minutes as shown in figure 18. The peak is relatively sharp, and it is significantly useful for distinguishing the starting materials from the conjugated product.

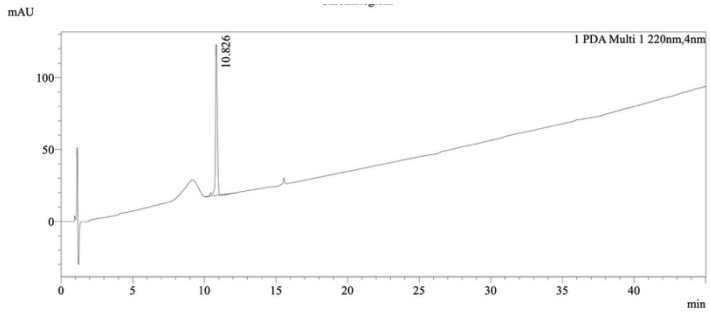

Figure 19: *Individual run of FNA-S-ACooP; retention time observed at t_R = 10.83 minutes*

The individual HPLC run was performed with m-carborane carboxylic acid stock solution, and it showed a major chromatographic peak at t_R = 27.95 minutes. This retention time is longer compared to FNA-S-ACooP which suggested more hydrophobic nature of carborane contained compounds.

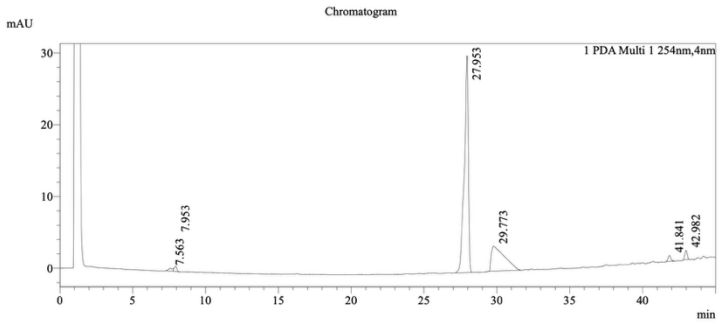

Figure 20: *Individual run of m-carborane carboxylic acid stock solution; retention time observed at t_R = 27.95 Minutes*

There was a minor peak broadening observed at t_R = 29.77 minutes, and several facts can be indicated as reason for this. One of the major reasons is the hydrophobic interaction with the column, presence of multiple closely related species, partially oxidised materials, and the gradient effect. Since the HPLC run time is 45 minutes the gradient changes near elution and this effects slightly stretched or distort late eluting peaks.

The reaction mixture was analysed immediately after mixing the starting materials and subsequent time points at 25 minutes and the 50 minutes. This analysis was particularly useful to observe the gradual changes in the chromatographic profile. The peak intensity was observed in figure 20 over time and this suggesting progressive formation of conjugated species during the coupling reaction.

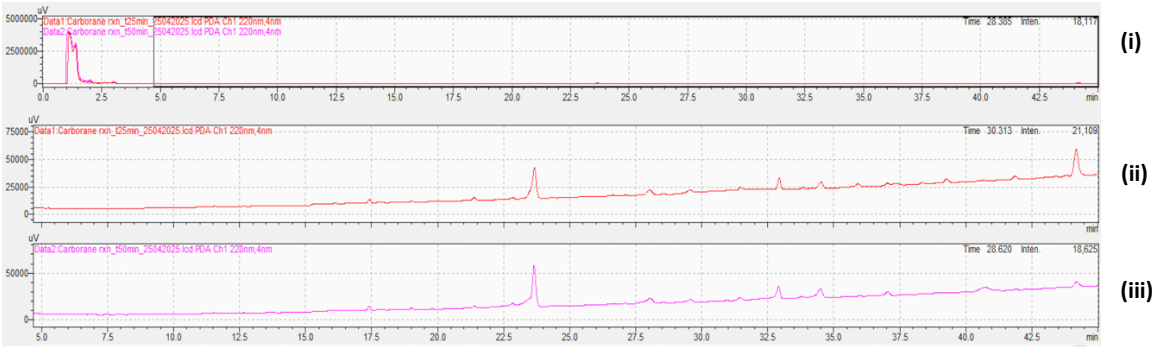

Figure 21: *Time point comparison of chromatograms of carborane-N-FNA-S-ACooP at 0 min, 25 min, 50 min;* ***(i)****chromatogram immediately after mixing starting materials* ***(ii)****chromatogram after 25 minutes of reaction time, materials* ***(iii)****chromatogram after 50 minutes of reaction time*

The above chromatograms supported to investigate the gradual formation of the analyte during the reaction and increasing concentration of product over time. The HPLC run time was fairly extended up to 45 minutes to ensure the elution of highly hydrophobic compounds and it allowed to monitor the late eluting hydrophobic conjugated moieties formed during the reaction.

QC chromatogram of the conjugated product illustrated in figure 22. The retention time recorded at t_R = 27.90 minutes, and it is closer to the carborane retention region compared to FNA-S-ACooP. This observation consistent with increase hydrophobicity following conjugation with the carborane cluster.

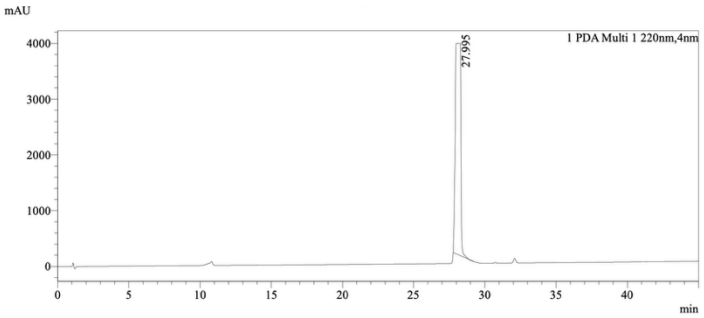

Figure 22: QC chromatogram of the isolated compound from the *carborane-N-FNA-S-ACooP synthesis; retention time recorded at t_R = 27.9 minutes.*

5.2.2 Characterisation of carborane-N-FNA-S-ACooP by HRMS

HRMS analysis was conducted for characterisation of the carborane-N-FNA-S-ACooP conjugation product following purification of the analyte with high mass positive analysis method. The total ion chromatogram showed a dominant chromatographic peak at 3.11 minutes along with several other lower intensity peaks observed with closer and nearby retention times (eg: t_R = 2.88 min, 3.28 min). Presence of multiple lower intensity chromatographic signals reveal formation of side products, impurities, incomplete conjugation products formed during the reaction etc.

The expected protonate molecular ion for carborane-N-FNA-S-ACooP should be theoretically $[M+ H]^+$ = 1140. 34231 which is clearly not observed in the spectra. It was observed some ions within the lower m/ z region which are corresponding with mass spectra. A well-defined ion which corresponding to the theoretical protonated mass of the analyte could not be verified with the analytical conditions applied. In figure 22, most of the ions observed with current spectra, due to fragmented ions and adducts which are originated during the ESI. Even though it was not enough evident to prove or to identify the definitive structural confirmation of the carborane peptide conjugation with the HRMS analysis, it was able to observe the progress of new conjugated compound with the chromatographic features obtained from HPLC analysis.

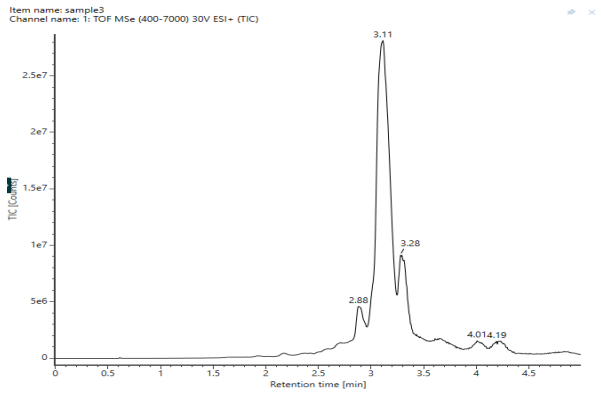

Figure 23: (i) *Total ion chromatogram (TIC) of carborane-N-FNA-S-ACooP;*

The following fragmentation ions and adducts are corresponded with the major peaks observed MS spectra, which is illustrated in figure 6, (i) and (ii) in the appendices.

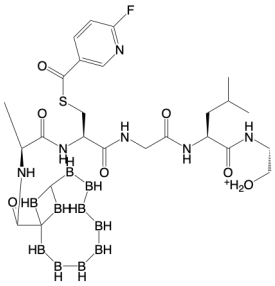

m/z 687

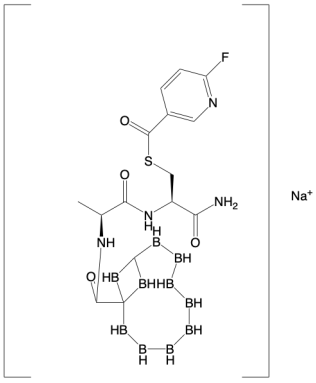

m/z 502

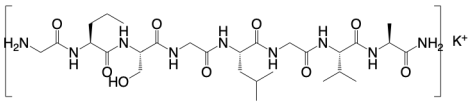

m/z 688

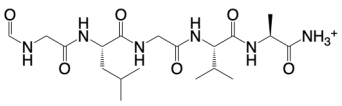

m/z 433

Figure 24: *Possible fragmentation ions and m/z values of carborane-N-FNA-S-ACooP corresponds with* ***(ii)*** *and* ***(iii)*** *spectra in figure 15*

The direct conjugation between carborane and peptide have been impacted by some reasons. The possibilities such as the unavailability and reduced accessibility of the free amino terminal of the peptide as the purification peptide has been performed with TFA and it led to strong ion pairing and formed a salt in the free amino end which has diminished the nucleophilicity. Further, the carborane moiety itself is a highly hydrophobic and it resulted poor solubility with the coupling medium (HATU in this case) and it has

mitigated the tendency of effective molecular interaction between reactants. On the other hand, there is a probability of inadequate activation of m-carborane carboxylic acid by HATU. This insufficient activation between carborane moiety and coupling medium led to hydrolysis of activated intermediate and also competing with side reaction could be reason for the failure of the direct carboane-peptide conjugation and the targeted product. There is another possible limitation could be the steric hindrance and the limited compatibility between the carborane cluster and the peptide backbone environment. In order to identify the analyte further, it is required to use analytical methods such as NMR analysis and tandem mass spectrometry etc. In this analysis it was suggested that further analytical optimisation is needed even with the purification process as well as the reaction conditions, coupling agents and the conjugation strategies to improve the comprehensive confirmation of the target compound.

5.3 Synthesis of FNA-S-ACooP-N-PEG$_2$-N$_3$

FNA-S-A-CooP-N-PEG$_2$-N$_3$ was synthesized successfully with an overall yield of 56.8% as illustrated in figure 25.

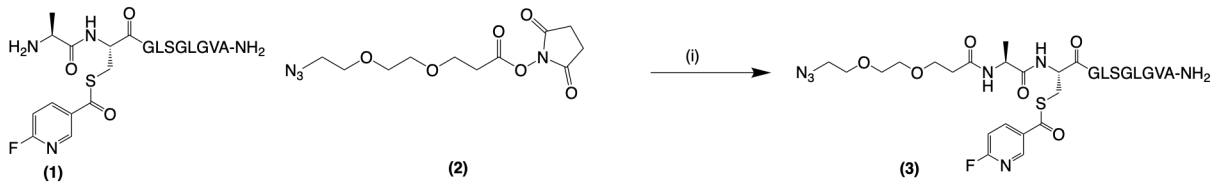

Figure 25: *Synthesis of FNA-S-A-CooP-N-PEG$_2$-N$_3$; **(1)** FNA-S-ACooP **(2)** Azido PEG$_2$-NHS ester **(3)** carborane-N-PEG$_2$-N$_3$; (i) borate buffer 90mM, pH 8.6, 3 hours at RT*

NHS ester mediated coupling reaction is taking place in between the reactants FNA-S-A-CooP **(1)** and Azido PEG$_2$-NHS ester **(2)** to form the conjugated product FNA-S-A-CooP-N-PEG$_2$-N$_3$ **(3)**. In this reaction, FNA-S-A-CooP **(1)** contributes as the nucleophile, and the target of the nucleophilic reaction is the activated carbonyl carbon of Azido PEG$_2$-NHS ester **(2).** During this reaction, nucleophilic acyl substitution occurs and followed by yielding of stable amide bond and subsequent elimination of N-hydroxysuccinamide (NHS) takes place as the leaving group[60]. As the reaction conditions it was provided a mildly basic pH (8.6) environment because NHS esters are favourable in reacting with amines under mild alkaline pH conditions [61] and this contributes to maintaining the deprotonated and nucleophilic form of amino group and led to efficient coupling reaction.

The aim of PEGylation in this reaction was to enhance the physiochemical and biological properties of the peptide conjugate comparative to direct carborane peptide conjugation while improving the solubility and the overall flexibility of the conjugated system.

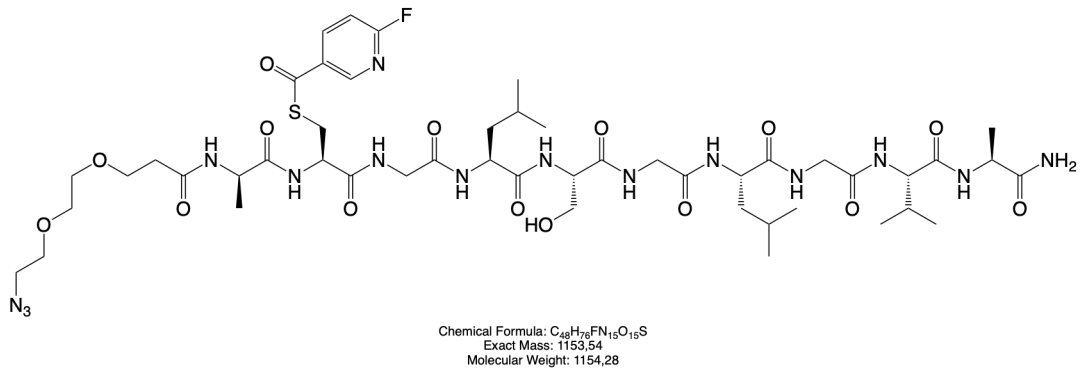

Figure 26: *Expanded molecular structure of FNA-S-A-CooP-N-PEG$_2$-N$_3$*

5.3.1 Characterisation of FNA-S-ACooP-N-PEG$_2$-N$_3$ by HPLC and HRMS analysis

HPLC runs were performed with the reaction mixture and get collected all the chromatographic peaks considered or potentially corresponding to the targeted analyte in order to determine the retention time. The chromatogram in figure 27 shows all the chromatographic peaks that are interested and collected.

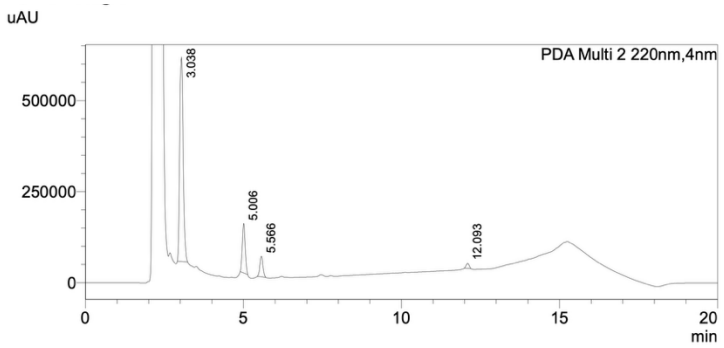

Figure 27: *HPLC chromatogram of FNA-S-A-CooP-N-PEG$_2$-N$_3$ reaction mixture eluted with TFA; four fractions were collected with following retention times t_R = 3.04 min, 5.01 min, 5.57 min, and 12.01 min*

Retention times of the starting materials also observed with HPLC analysis, they were t_R = 3.21 min for Azido PEG$_2$-NHS ester and t_R = 5.11 min for FNA-S-A-CooP. Preliminary identifications were supported with HRMS analysis. The theoretical m/z value is 1153.53. The fraction collected at 5.57 min as shown in figure 27 was corresponded with the resemblance structure of FNA-S-A-CooP-N-PEG$_2$-N$_3$ at m/z 1127. 52183. But the analyse sample showed relatively low peak intensities and it was not enough evidence to make a claim that the desired analyte present in the sample. Figure 28 illustrated the MS spectra with relative abundance of the analyte. There were sufficient data to confirm that the fractions collected at t_R = 3.0038 min, and t_R = 5.006 as shown in figure 27 were corresponded with Azido PEG$_2$-NHS ester and for FNA-S-A-CooP respectively with HRMS data.

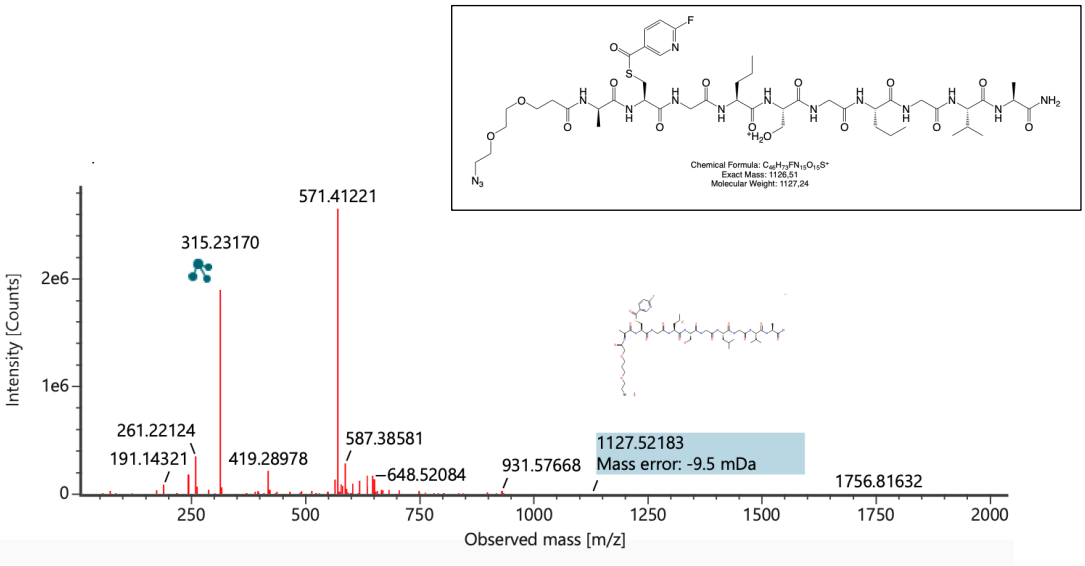

Figure 28: *MS spectra of FNA-S-A-CooP-N-PEG$_2$-N$_3$ eluted with TFA during the fraction collection of HPLC analysis*

It was required to develop a method for analyte detection while improving conjugation efficiency of PEG-peptide bond. It was clearly identified that the conjugation has mitigated due to low accessibility of terminal amine of FNA-S-A-CooP as a result of purified with TFA. Hence, further analytical investigations were subsequently employed with HCOOH purified FNA-S-A-CooP and the reaction mixture also was eluted with HCOOH accordingly. Figure 29 represented the HPLC chromatogram of the reaction mixture when eluted with HCOOH.

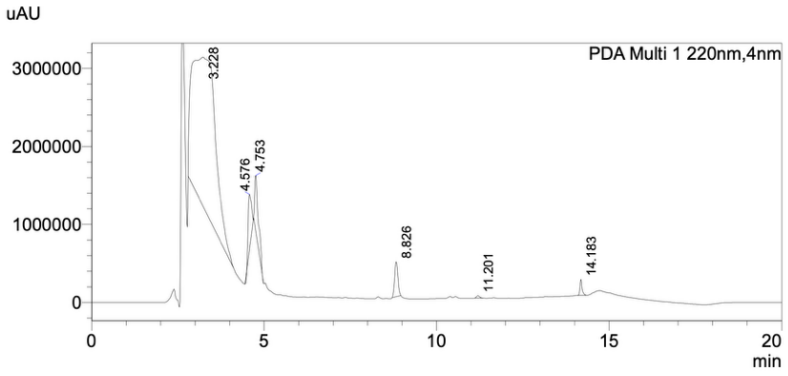

Figure 29*: HPLC chromatogram of FNA-S-A-CooP-N-PEG$_2$-N$_3$ reaction mixture eluted with HCOOH*

Retention time of the starting materials were identified with individual HPLC runs. According to the figure 22 retention the time t_R = 3.228 min and t_R = 4.576 min were corresponded with Azido PEG$_2$-NHS ester and FNA-S-A-CooP respectively. The HPLC flowrate was slowed down (3.5 mL/min) as mentioned in the method section to collect the analyte sample as reported at retention time of t_R = 4.75 min which has presented in figure 29.

Qualitative structural characterisation and compound identification of the analyte FNA-N-ACooP-N- PEG$_2$-NHS ester was performed with HRMS. In this analysis it was focused the fragmentation patterns, chromatographic peaks and comparison of expected exact mass of the analyte and the starting materials as

well. Figure 30 shows the results of HRMS analysis which revealed major chromatographic peak at retention time of t_R = 2.47 minutes. The theoretical monoisotopic mass of FNA-S-ACooP-N- PEG_2-NHS ester was m/z 1153.53 for molecular ion [M + H]$^+$. The major peak observed at m/z 1176.53311 likely correspond to a sodium adduct [M + Na]$^+$ generated during positive ESI, and the retention time of chromatogram recorded as t_R = 2.47 minutes as shown in figure 31.

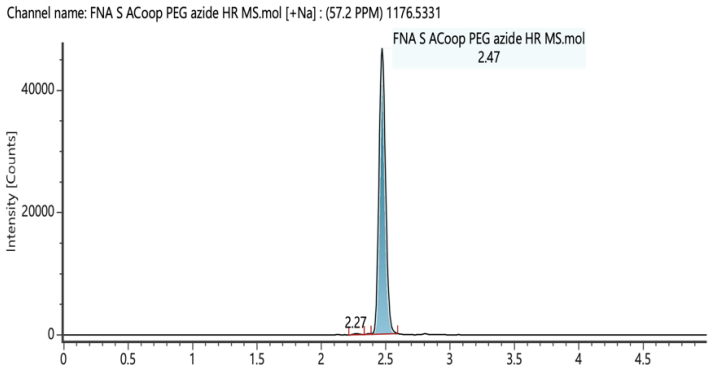

Figure 30: *Extracted chromatogram of HCOOH purified FNA-S-ACooP-N- PEG_2-NHS indicating the major chromatographic peak at t_R = 2.47 minutes*

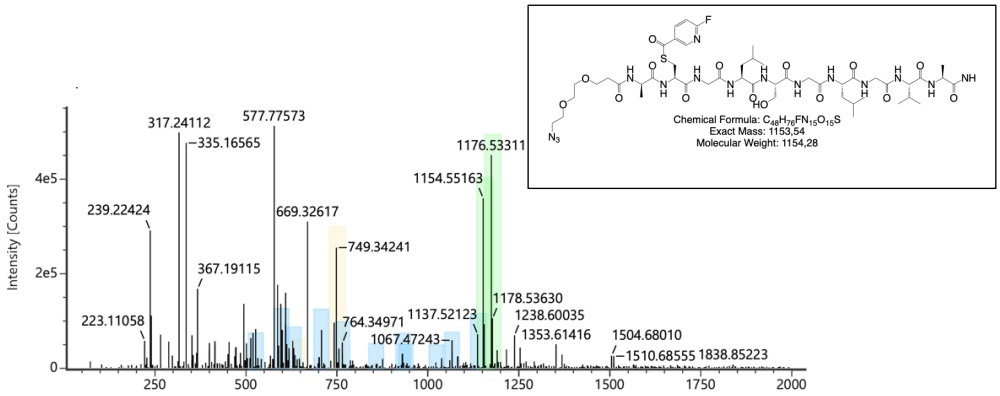

Figure 31: *Extracted TIC of FNA-S-ACooP-N- PEG_2-NHS eluted with HCOOH indicating the major peak at m/z 1176.*53311

Simultaneously, the fractions, collected as starting materials during HPLC semi preparative purification also subjected to HRMS analysis to verify further and confirm the identity of each starting material. The results are as follows. Figure 32 shows the results of HRMS analysis which revealed major chromatographic peak at retention time of t_R = 2.11 minutes. The theoretical monoisotopic mass of FNA-N-ACooP **(3)** was m/z 969.462 for the singly protonated molecular ion [M + H]$^+$ whereas the observed m/ z was 969.46684 and doubly charged ions of FNA-N-ACooP [M + 2H]$^{2+}$ at m/z 481.25489. Figure 33 shows the results of HRMS analysis which revealed major chromatographic peak at retention time of Azido PEG_2-NHS ester t_R = 1.84 minutes. The theoretical monoisotopic mass of was m/z 300.11 for the singly protonated molecular ion [M + H]$^+$ whereas the observed m/ z was 323.09699.

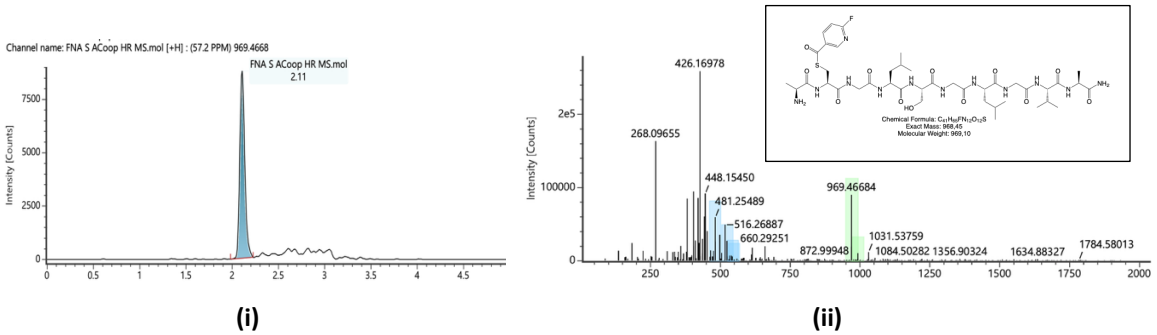

Figure 32: (i) *Extracted chromatogram of HCOOH purified FNA-S-A-CooP indicating the major chromatographic peak at t_R = 2.11 minutes;* ***(ii)*** *TIC of HCOOH purified FNA-S-A-CooP*

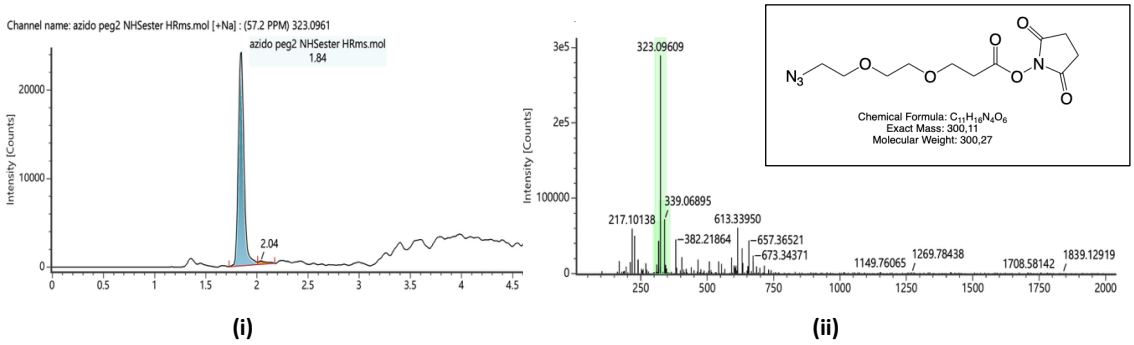

Figure 33: (i) *Extracted chromatogram of HCOOH purified Azido-PEG2-NHS ester indicating the major chromatographic peak at t_R = 1.84 minutes;* ***(ii)*** *TIC of HCOOH purified Azido PEG HNS ester*

5.3.2 Characterisation of FNA-S-ACooP-N-PEG_2-N_3 by NMR analysis

The ^{1}H NMR analysis for FNA-S-ACooP-N-PEG_2-N_3 was success even though the signal demonstrated low intensities. It was able to identify the signals correspond with peptide structure, PEG linker, as well as the aromatic region of fluoronicotinic moiety. Majority of signals from the PEG methylene protons observed with the region of 3ppm- 4ppm indicating successful incorporation of PEG linker to the peptide backbone. It was able to identify the terminal amide in within 8ppm-10 ppm, and it was down fielded.

HSQC did not yield the expected results as the ^{13}C signals were able to identify poorly.

5.4 Synthesis of carborane-propargyl-PEG$_3$ conjugation

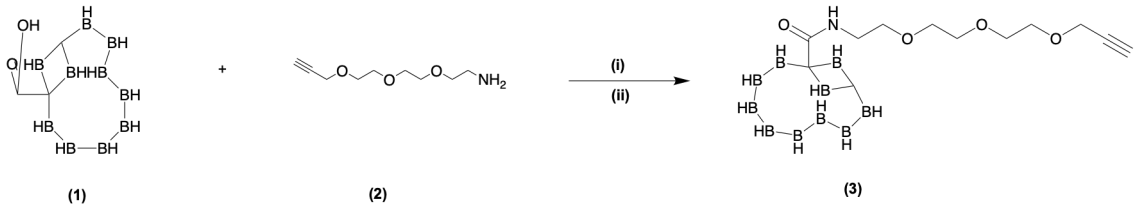

Figure 34: *Synthesis of carborane-- propargyl- PEG$_3$ conjugation: (1) m-carborane-carboxylic acid; (2) propargyl-PEG3-amine; (3) carborane- propargyl- PEG3 conjugation product; (i) HATU; (ii) DIPEA*

In this research, the synthesis step prior to the last step was the carborane- propargyl-PEG$_3$ conjugation reaction. The resulted product was a PEGylated carborane contain intermediate. The reaction was proceeded through amide bond formation between m-carborane carboxylic acid and the terminal amine group of propargyl-PEG$_3$ amine. Nucleophilic acyl substitution reaction takes place, and the activated carboxylic acid derivative intermediate reacts with nucleophilic amino terminus of the PEG linker in the HATU mediated coupling conditions, in the presence of DIPEA as the base. In this reaction strategy, the introduction of the PEG$_3$ linker[62] was expected to improve develop and improve hydrophilicity and to enhance the flexibility of carborane conjugated system. In contrast, PEG spacer reduces the steric hindrance between bulky carborane cluster and the biomolecular conjugate. This contributes to facilitate coupling efficiency and the molecular accessibility.

5.4.1 Characterisation of carborane-N-propargyl-PEG$_3$ conjugation

Characterisation was completed fundamentally with HPLC analysis and found the retention time of the target analyte was t_R = 27.96 minutes as shown in figure 35.

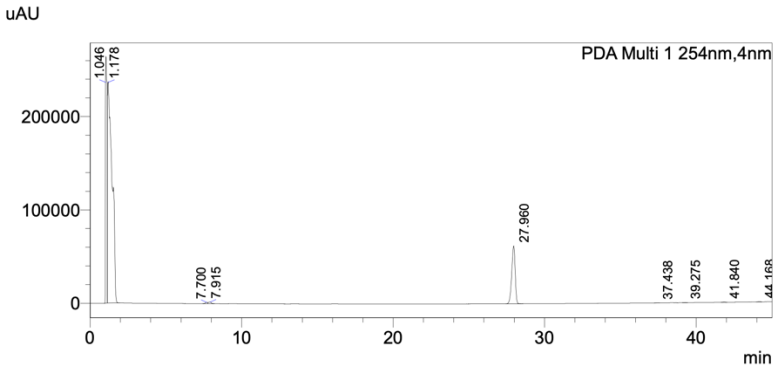

Figure 35: *HPLC chromatogram of carborane-N-propargyl-PEG$_3$: retention time of the analyte recorded as t_R = 27.96 minutes*

The analyte was followed by the HRMS analysis as the next step of proving the exact compound. DIPEA was removed as it ionizes strongly in the mass spectrum and further suppresses the analyte ionisation. The HRMS analysis was carried out in low mass positive ionization mode. The theoretical molecular ion corresponding to the target analyte at m/ z 359.29 could not be precisely identify under the analytical conditions employed. Several fragmentation related ions were able to observe, and they showed reasonable agreements with the experimental MS data obtained at m/z 190.20, m/z 253.21, m/z 166.06 and m/z 188.13.

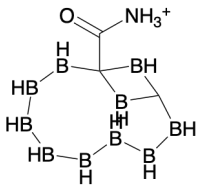

m/z 190.20

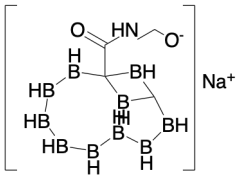

m/z 253.21

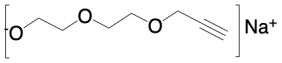

m/z 166.06

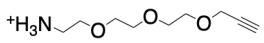

m/z 188.13

Figure 36: *The proposed fragment ions of carborane- propargyl-PEG$_3$ correspond with fragment species during ESI*

Conclusive evidence of the target analyte was not possibly established solely based on HRMS data as due to complexity of the obtained spectra, but from the analysis it was able to interpret several ions as shown in figure 36 that are corresponding with fragment species, adduct associated ions or partially degraded products formed during ESI. Further, it is known to be relatively complicated the fragmentation of carborane conjugates compounds[63,64] also another possible reason for this observation. However, the associated complications could be due to cleavages of amide linkages, partial fragmentation of the PEG chain, and formation of boron cluster containing fragmentation ions.

5.5 Synthesis of carborane-N-FNA-S-ACooP

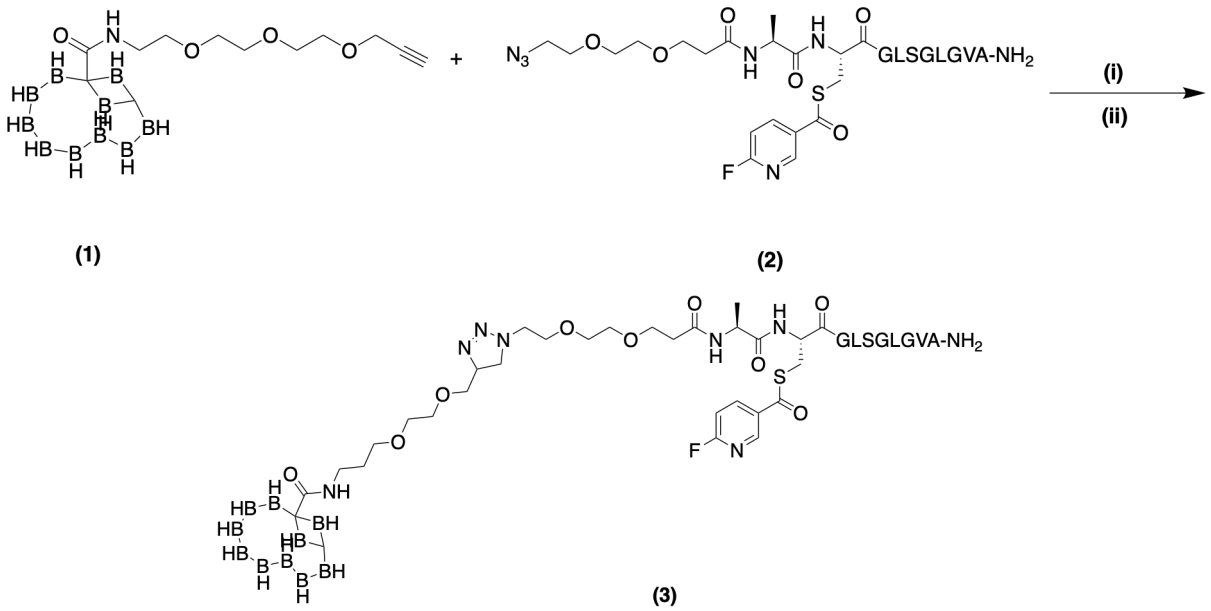

Figure 37: *Synthesis of carborane-N-FNA-S-ACooP**(3)**: **(1)** carborane-N-propargyl-PEG$_3$; **(2)** FNA-S-ACooP-N-PEG$_2$; **(i)** Copper sulphate ($CuSO_4$); **(ii)**Sodium ascorbate ($C_6H_7NaO_6$)*

Figure 37 shows the final target compound of the research work carborane-N-FNA-S-ACooP **(3).** Carborane-N-FNA-S-ACooP **(3)** is a carborane functionalised peptide conjugate which was expected to be synthesised through a biorthogonal click reaction strategy via 1,3 dipolar cycloadditions. The coupling between the two pre prepared conjugated products which are, carborane-N-propargyl-PEG$_3$**(1)** and FNA-S-ACooP-N-PEG$_2$-N$_3$ **(2)** takes place using copper catalysed azide alkyne cyclo addition (CuAAC) [50,65]conditions in the presence of copper sulphate **(i)** and sodium ascorbate**(ii).**

A total of 1.80 mg of purified FNA-S-ACooP was isolated corresponding to the yield of 62.3%. From this starting material 0.64 mg of purified FNA-S-ACooP-N-PEG$_2$-N$_3$ was obtained corresponding to the yield of 56.8%. However, the carborane-propargyl-PEG$_3$ conjugate could not be isolated in a sufficient pure form for complete characterisation. As a result, the quantity of material available was not adequate for investigating the final reaction step which is the synthesis of carborane-N-FNA-S-ACooP **(3).**

Therefore, as constrains which are affected for limitations and the target product could not be achieve, could be specified as insufficient amount of synthesized starting materials, synthesized conjugated products and inadequate optimization of coupling conditions. It is necessary to develop further optimisation studies to improve the efficiency and reproducibility of the conjugation process.

6 Conclusion

In summary, the aim of the research work was on the development of the 18F- labelled carborane-peptide conjugates based on the biomolecule FNA-S-ACooP. It was derived from the previous studies with the objectives of optimizing of sulphur linked peptide conjugation system through S acylation strategies. The previous studies in accordance with N acylation; and compared to conventional N acylation, introduction of S acylation provides modified physiochemical and conjugation properties that could be beneficial for peptide based radiopharmaceutical development. The modifications and the enhancement of boron rich carborane moieties along with the biomolecule FNA-S-ACooP was particular interest due to their potential applications in BNCT, because selective delivery of boron rich compounds to tumour tissue is highly crucial. Hence, the development and refinement of PEGylated carborane-peptide conjugates indicate a promising strategy towards establishment of targeting systems for future PET and BNCT related applications.

The first goal of this thesis work was to synthesise direct carborane -peptide conjugation product. Therefore, the biomolecule FNA-S-ACooP was able to synthesis successfully and afforded with 62.3% and the characterisation also was progressed with HPLC, HRMS and NMR analytical approaches. The results of the purification strategies demonstrated that the purification conditions facilitate significantly in the conjugation efficiency of the subsequent steps. Switching the HPLC solvent from TFA to HCOOH was benefited and affected the overall conjugation efficiency and analytical accessibility and detectability of peptide system due to availability of free amino terminus of the peptide. However, the first approach which is direct carborane-peptide conjugation could not be achieved as planned due to steric hindrance of the carborane moiety and the limited compatibility of the carborane-peptide conjugate.

The next strategy was the coupling of carborane-peptide conjugation via a PEGylated linker. The PEG compound used; to achieve this target was Azido PEG_2-NHS ester and it was able to be synthesised FNA-S-ACooP-N- PEG_2-N_3; afforded with 76.8% and the characterisation also was proceeded with HPLC, HRMS and NMR analytical approaches. It was also revealed the necessity of purifying the analyte with HCOOH than TFA is significantly important to elevate the conjugation efficiency. However, it is crucial to optimise the PEGylation conditions, purification parameters, and the stoichiometry of starting materials and the effect of excess starting materials and the limiting agents also remain important. For example, excess amount of azido PEG_2 NHS ester may cause several complications in the HPLC purification. Specially NHS esters are highly susceptible to hydrolysis in aqueous conditions as well as a reason to form multiple nucleophilic sites. The carborane contain moiety was not possible to synthesised as the characterisation step could not achieve with HRMS analysis. The complexity of carborane fragmentated ions during ESI was the reason. Therefore, it is required to optimise the LC-MS conditions along with another MS strategy such as MALDI or triple quadruple method would have been beneficial including optimal convoluted voltage. Final target product, carborane-N-FNA-S-ACooP could not be accomplished due to challenges in characterising conclusively the previous intermediate in the reaction scheme. The synthesis of carborane- propargyl-PEG_3 conjugation reaction is the most important step that aids the conjugation of carborane moiety to the final target compound. Therefore, it could benefit from further optimisation of the reaction condition and

develop a new strategy to resynthesis the compound. The overall finding of this research possesses the potential for a cold tracer which is a peptide-based conjugation platform in the PET chemistry. Further systemic optimisation and optimised analytical characterisation will be necessary to accomplish the desired outcome and to obtain the definitive confirmation of the final carborane- peptide conjugate.

7 Reference

(1) Louis, D. N.; Perry, A.; Wesseling, P.; Brat, D. J.; Cree, I. A.; Figarella-Branger, D.; Hawkins, C.; Ng, H. K.; Pfister, S. M.; Reifenberger, G.; Soffietti, R.; von Deimling, A.; Ellison, D. W. The 2021 WHO Classification of Tumors of the Central Nervous System: A Summary. Neuro Oncol 2021, 23 (8), 1231–1251. https://doi.org/10.1093/neuonc/noab106.

(2) Bray, F.; Laversanne, M.; Sung, H.; Ferlay, J.; Siegel, R. L.; Soerjomataram, I.; Jemal, A. Global Cancer Statistics 2022: GLOBOCAN Estimates of Incidence and Mortality Worldwide for 36 Cancers in 185 Countries. CA Cancer J Clin 2024, 74 (3), 229–263. https://doi.org/10.3322/caac.21834.

(3) Deeken, J. F.; Löscher, W. The Blood-Brain Barrier and Cancer: Transporters, Treatment, and Trojan Horses. Clin Cancer Res 2007, 13 (6), 1663–1674. https://doi.org/10.1158/1078-0432.CCR-06-2854.

(4) Stupp, R.; Hegi, M. E.; Mason, W. P.; van den Bent, M. J.; Taphoorn, M. J. B.; Janzer, R. C.; Ludwin, S. K.; Allgeier, A.; Fisher, B.; Belanger, K.; Hau, P.; Brandes, A. A.; Gijtenbeek, J.; Marosi, C.; Vecht, C. J.; Mokhtari, K.; Wesseling, P.; Villa, S.; Eisenhauer, E.; Gorlia, T.; Weller, M.; Lacombe, D.; Cairncross, J. G.; Mirimanoff, R.-O.; European Organisation for Research and Treatment of Cancer Brain Tumour and Radiation Oncology Groups; National Cancer Institute of Canada Clinical Trials Group. Effects of Radiotherapy with Concomitant and Adjuvant Temozolomide versus Radiotherapy Alone on Survival in Glioblastoma in a Randomised Phase III Study: 5-Year Analysis of the EORTC-NCIC Trial. Lancet Oncol 2009, 10 (5), 459–466. https://doi.org/10.1016/S1470-2045(09)70025-7.

(5) Dillemuth, P.; Karskela, T.; Ayo, A.; Ponkamo, J.; Kunnas, J.; Rajander, J.; Tynninen, O.; Roivainen, A.; Laakkonen, P.; Airaksinen, A. J.; Li, X.-G. Radiosynthesis, Structural Identification and in Vitro Tissue Binding Study of [18F]FNA-S-ACooP, a Novel Radiopeptide for Targeted PET Imaging of Fatty Acid Binding Protein 3. EJNMMI radiopharm. chem. 2024, 9 (1), 16. https://doi.org/10.1186/s41181-024-00245-3.

(6) Dillemuth, P.; Lövdahl, P.; Karskela, T.; Ayo, A.; Ponkamo, J.; Liljenbäck, H.; Paunonen, S.; Kunnas, J.; Rajander, J.; Tynninen, O.; Rosenholm, J. M.; Roivainen, A.; Laakkonen, P.; Airaksinen, A. J.; Li, X.-G. Switching the Chemoselectivity in the Preparation of [^{18} F]FNA- N -CooP, a Free Thiol-Containing Peptide for Targeted Positron Emission Tomography Imaging of Fatty Acid Binding Protein 3. Mol. Pharmaceutics 2024, 21 (8), 4147–4156. https://doi.org/10.1021/acs.molpharmaceut.4c00546.

(7) Jyothi, V. G. S. S.; Kommineni, N. Peptide Conjugated Boron Neutron Capture Therapy for Enhanced Tumor Targeting. Nanotheranostics 2024, 8 (4), 458–472. https://doi.org/10.7150/ntno.95251.

(8) Yang, Q.; Dai, Q.; Bao, X.; Zhou, Y.; Lu, Y.; Zhong, H.; Wu, L.; Guo, Y.; Liu, L.; Tan, X.; Xia, Y.; Han, M.; Wei, Q. Evaluation of a Tumor-Targeting Oligosaccharide Nanosystem in BNCT on an Orthotopic Hepatocellular Carcinoma Model. Mol. Pharmaceutics 2023, 20 (2), 1025–1038. https://doi.org/10.1021/acs.molpharmaceut.2c00771.

(9) Wiebe, L. I. Radionuclides, Radiotracers and Radiopharmaceuticals for in Vivo Diagnosis. Radiation Physics and Chemistry (1977) 1984, 24 (3–4), 365–372. https://doi.org/10.1016/0146-5724(84)90073-6.

(10) Shetty, H. U.; Morse, C. L.; Zhang, Y.; Pike, V. W. Characterization of Fast-Decaying PET Radiotracers Solely through LC-MS/MS of Constituent Radioactive and Carrier Isotopologues. EJNMMI Res 2013, 3 (1), 3. https://doi.org/10.1186/2191-219X-3-3.

(11) Almuhaideb, A.; Papathanasiou, N.; Bomanji, J. 18F-FDG PET/CT Imaging in Oncology. Ann Saudi Med 2011, 31 (1), 3–13. https://doi.org/10.4103/0256-4947.75771.

(12) Lameka, K.; Farwell, M. D.; Ichise, M. Positron Emission Tomography. Handb Clin Neurol 2016, 135, 209–227. https://doi.org/10.1016/B978-0-444-53485-9.00011-8.

(13) Bailey, D. L.; Antoch, G.; Bartenstein, P.; Barthel, H.; Beer, A. J.; Bisdas, S.; Bluemke, D. A.; Boellaard, R.; Claussen, C. D.; Franzius, C.; Hacker, M.; Hricak, H.; la Fougère, C.; Gückel, B.; Nekolla, S. G.; Pichler, B. J.; Purz, S.; Quick, H. H.; Sabri, O.; Sattler, B.; Schäfer, J.; Schmidt, H.; van den Hoff, J.; Voss, S.; Weber, W.; Wehrl, H. F.; Beyer, T. Combined PET/MR: The Real Work Has Just Started. Summary Report of the Third International Workshop on PET/MR Imaging; February 17-21, 2014, Tübingen, Germany. Mol Imaging Biol 2015, 17 (3), 297–312. https://doi.org/10.1007/s11307-014-0818-0.

(14) Shaikh, S. PET-CT Imaging and Applications. In Computed-Tomography (CT) Scan; R. Gharieb, R., Ed.; IntechOpen, 2022. https://doi.org/10.5772/intechopen.103975.

(15) Omami, G.; Tamimi, D.; Branstetter, B. F. Basic Principles and Applications of (18)F-FDG-PET/CT in Oral and Maxillofacial Imaging: A Pictorial Essay. Imaging Sci Dent 2014, 44 (4), 325–332. https://doi.org/10.5624/isd.2014.44.4.325.

(16) Omami, G.; Tamimi, D.; Branstetter, B. F. Basic Principles and Applications of (18)F-FDG-PET/CT in Oral and Maxillofacial Imaging: A Pictorial Essay. Imaging Sci Dent 2014, 44 (4), 325–332. https://doi.org/10.5624/isd.2014.44.4.325.
(17) Shukla, A.; Kumar, U. Positron Emission Tomography: An Overview. J Med Phys 2006, 31 (1), 13. https://doi.org/10.4103/0971-6203.25665.
(18) Chinn, G.; Levin, C. S. A Maximum NEC Criterion for Compton Collimation to Accurately Identify True Coincidences in PET. IEEE Trans. Med. Imaging 2011, 30 (7), 1341–1352. https://doi.org/10.1109/TMI.2011.2113379.
(19) Shibuya, K.; Yoshida, E.; Nishikido, F.; Suzuki, T.; Tsuda, T.; Inadama, N.; Yamaya, T.; Murayama, H. Annihilation Photon Acollinearity in PET: Volunteer and Phantom FDG Studies. Phys. Med. Biol. 2007, 52 (17), 5249–5261. https://doi.org/10.1088/0031-9155/52/17/010.
(20) Oliver, J. F.; Rafecas, M. Modelling Random Coincidences in Positron Emission Tomography by Using Singles and Prompts: A Comparison Study. PLoS ONE 2016, 11 (9), e0162096. https://doi.org/10.1371/journal.pone.0162096.
(21) Crișan, G.; Moldovean-Cioroianu, N. S.; Timaru, D.-G.; Andrieș, G.; Căinap, C.; Chiș, V. Radiopharmaceuticals for PET and SPECT Imaging: A Literature Review over the Last Decade. Int J Mol Sci 2022, 23 (9), 5023. https://doi.org/10.3390/ijms23095023.
(22) Phelps, M. E. PET: The Merging of Biology And.
(23) Townsend, D. W. Multimodality Imaging of Structure and Function. Phys. Med. Biol. 2008, 53 (4), R1–R39. https://doi.org/10.1088/0031-9155/53/4/R01.
(24) Townsend, D. W. Multimodality Imaging of Structure and Function. Phys. Med. Biol. 2008, 53 (4), R1–R39. https://doi.org/10.1088/0031-9155/53/4/R01.
(25) Cherry, S. R.; Jones, T.; Karp, J. S.; Qi, J.; Moses, W. W.; Badawi, R. D. Total-Body PET: Maximizing Sensitivity to Create New Opportunities for Clinical Research and Patient Care. J Nucl Med 2018, 59 (1), 3–12. https://doi.org/10.2967/jnumed.116.184028.
(26) Lapi, S. E.; Welch, M. J. A Historical Perspective on the Specific Activity of Radiopharmaceuticals: What Have We Learned in the 35 Years of the ISRC? Nuclear Medicine and Biology 2012, 39 (5), 601–608. https://doi.org/10.1016/j.nucmedbio.2011.11.005.
(27) Coenen, H. H.; Gee, A. D.; Adam, M.; Antoni, G.; Cutler, C. S.; Fujibayashi, Y.; Jeong, J. M.; Mach, R. H.; Mindt, T. L.; Pike, V. W.; Windhorst, A. D. Consensus Nomenclature Rules for Radiopharmaceutical Chemistry — Setting the Record Straight. Nuclear Medicine and Biology 2017, 55, v–xi. https://doi.org/10.1016/j.nucmedbio.2017.09.004.
(28) Sergeev, M.; Lazari, M.; Morgia, F.; Collins, J.; Javed, M. R.; Sergeeva, O.; Jones, J.; Phelps, M. E.; Lee, J. T.; Keng, P. Y.; Van Dam, R. M. Performing Radiosynthesis in Microvolumes to Maximize Molar Activity of Tracers for Positron Emission Tomography. Commun Chem 2018, 1 (1), 10. https://doi.org/10.1038/s42004-018-0009-z.
(29) Gmez-Vallejo, V.; Gaja, V.; Koziorowski, J.; Llop, J. Specific Activity of 11C-Labelled Radiotracers: A Big Challenge for PET Chemists. In Positron Emission Tomography - Current Clinical and Research Aspects; Hsieh, C.-H., Ed.; InTech, 2012. https://doi.org/10.5772/31491.
(30) Richter, S.; Wuest, F. 18F-Labeled Peptides: The Future Is Bright. Molecules 2014, 19 (12), 20536–20556. https://doi.org/10.3390/molecules191220536.
(31) Kumar, K.; Ghosh, A. 18F-AlF Labeled Peptide and Protein Conjugates as Positron Emission Tomography Imaging Pharmaceuticals. Bioconjug Chem 2018, 29 (4), 953–975. https://doi.org/10.1021/acs.bioconjchem.7b00817.
(32) Clark, J. C.; Silvester, D. J. A Cyclotron Method for the Production of Fluorine-18. The International Journal of Applied Radiation and Isotopes 1966, 17 (3), 151–154. https://doi.org/10.1016/0020-708X(66)90039-1.
(33) Jacobson, O.; Kiesewetter, D. O.; Chen, X. Fluorine-18 Radiochemistry, Labeling Strategies and Synthetic Routes. Bioconjug Chem 2015, 26 (1), 1–18. https://doi.org/10.1021/bc500475e.
(34) Guillaume, M.; Luxen, A.; Nebeling, B.; Argentini, M.; Clark, J. C.; Pike, V. W. Recommendations for Fluorine-18 Production. International Journal of Radiation Applications and Instrumentation. Part A. Applied Radiation and Isotopes 1991, 42 (8), 749–762. https://doi.org/10.1016/0883-2889(91)90179-5.
(35) Remy, I.; Campbell-Valois, F. X.; Michnick, S. W. Detection of Protein–Protein Interactions Using a Simple Survival Protein-Fragment Complementation Assay Based on the Enzyme Dihydrofolate Reductase. Nat Protoc 2007, 2 (9), 2120–2125. https://doi.org/10.1038/nprot.2007.266.
(36) Zhuang, X.; Kunnas, J.; Ekwe, D.; Bakay, E.; Dillemuth, P.; Liljenbäck, H.; Iqbal, I.; Rajander, J.; Low, P. S.; Knuuti, J.; Rosenholm, J. M.; Saraste, A.; Roivainen, A.; Li, X.-G. [^{18} F]Fluoronicotinic-Acid-Conjugated

Folate as a Novel Candidate Positron Emission Tomography Tracer for Inflammation. ACS Omega 2026, 11 (1), 1898–1907. https://doi.org/10.1021/acsomega.5c10157.
(37) Dillemuth, P.; Ayo, A.; Zhuang, X.; Lövdahl, P.; Liljenbäck, H.; Kärnä, S.; Auchynnikava, T.; Kunnas, J.; Ponkamo, J.; Miner, M. W. G.; Rajander, J.; Rosenholm, J. M.; Roivainen, A.; Airaksinen, A. J.; Laakkonen, P.; Li, X.-G. Rapid Cleavage of 6-[18F]Fluoronicotinic Acid Prosthetic Group Governs BT12 Glioblastoma Xenograft Uptake: Implications for Radiolabeling Design of Biomolecules. EJNMMI radiopharm. chem. 2025, 10 (1), 40. https://doi.org/10.1186/s41181-025-00368-1.
(38) Dillemuth, P.; Ayo, A.; Airenne, T. T.; Lövdahl, P.; Bakay, E.; Zhuang, X.; Liljenbäck, H.; Paunonen, S. T.; Kunnas, J.; Filppu, P.; Rajander, J.; Johnson, M. S.; Roivainen, A.; Salminen, T. A.; Rosenholm, J. M.; Laakkonen, P.; Li, X.-G. Utilizing Monocarboxylate Transporter 1-Mediated Blood–Brain Barrier Penetration for Glioblastoma Positron Emission Tomography Imaging with 6-[^{18} F]Fluoronicotinic Acid. Mol. Pharmaceutics 2025, 22 (8), 4819–4830. https://doi.org/10.1021/acs.molpharmaceut.5c00457.
(39) Wang, S.; Zhang, Z.; Miao, L.; Li, Y. Boron Neutron Capture Therapy: Current Status and Challenges. Front. Oncol. 2022, 12, 788770. https://doi.org/10.3389/fonc.2022.788770.
(40) Jin, W. H.; Seldon, C.; Butkus, M.; Sauerwein, W.; Giap, H. B. A Review of Boron Neutron Capture Therapy: Its History and Current Challenges. International Journal of Particle Therapy 2022, 9 (1), 71–82. https://doi.org/10.14338/IJPT-22-00002.1.
(41) Luderer, M. J.; De La Puente, P.; Azab, A. K. Advancements in Tumor Targeting Strategies for Boron Neutron Capture Therapy. Pharm Res 2015, 32 (9), 2824–2836. https://doi.org/10.1007/s11095-015-1718-y.
(42) Murilla, R. M.; Edilo, G. G.; Budlayan, M. L. M.; Auxtero, E. S. Boron Delivery Agents in BNCT: A Mini Review of Current Developments and Emerging Trends. Nano TransMed 2025, 4, 100081. https://doi.org/10.1016/j.ntm.2025.100081.
(43) Lützenburg, T.; Neundorf, I.; Scholz, M. Direct Carborane-Peptide Conjugates: Synthesis and Evaluation as Non-Natural Lipopeptide Mimetics. Chem Phys Lipids 2018, 213, 62–67. https://doi.org/10.1016/j.chemphyslip.2018.03.009.
(44) Veronese, F. M.; Mero, A. The Impact of PEGylation on Biological Therapies. BioDrugs 2008, 22 (5), 315–329. https://doi.org/10.2165/00063030-200822050-00004.
(45) Vakhrushev, A. V.; Gruzdev, D. A.; Demin, A. M.; Levit, G. L.; Krasnov, V. P. Synthesis of Novel Carborane-Containing Derivatives of RGD Peptide. Molecules 2023, 28 (8), 3467. https://doi.org/10.3390/molecules28083467.
(46) Li, C.; Li, T.; Tian, X.; An, W.; Wang, Z.; Han, B.; Tao, H.; Wang, J.; Wang, X. Research Progress on the PEGylation of Therapeutic Proteins and Peptides (TPPs). Front. Pharmacol. 2024, 15, 1353626. https://doi.org/10.3389/fphar.2024.1353626.
(47) Veronese, F. M. Peptide and Protein PEGylation. Biomaterials 2001, 22 (5), 405–417. https://doi.org/10.1016/S0142-9612(00)00193-9.
(48) Beutick, S. E.; Vermeeren, P.; Hamlin, T. A. The 1,3-Dipolar Cycloaddition: From Conception to Quantum Chemical Design. Chemistry An Asian Journal 2022, 17 (17), e202200553. https://doi.org/10.1002/asia.202200553.
(49) Tron, G. C.; Pirali, T.; Billington, R. A.; Canonico, P. L.; Sorba, G.; Genazzani, A. A. Click Chemistry Reactions in Medicinal Chemistry: Applications of the 1,3-dipolar Cycloaddition between Azides and Alkynes. Medicinal Research Reviews 2008, 28 (2), 278–308. https://doi.org/10.1002/med.20107.
(50) Liang, L.; Astruc, D. The Copper(I)-Catalyzed Alkyne-Azide Cycloaddition (CuAAC) “Click” Reaction and Its Applications. An Overview. Coordination Chemistry Reviews 2011, 255 (23–24), 2933–2945. https://doi.org/10.1016/j.ccr.2011.06.028.
(51) Https://Www.Shimadzu.Com/an/Service-Support/Technical-Support/Analysis-Basics/Basic/What_is_hplc.Html.
(52) Kaur, P.; Vyas, M.; Verma, S. P.; Sahu, S. K. RP-HPLC Method Development and Validation for the Simultaneous Estimation of Piceatannol and -Arginine in Pharmaceutical Formulations. Current Pharmaceutical Analysis 2026, 22 (1), 66–73. https://doi.org/10.1016/j.cpan.2025.12.004.
(53) How Does High Performance Liquid Chromatography (HPLC) Work?
(54) Https://Www.Waters.Com/Nextgen/Us/En/Education/Primers/Beginner-s-Guide-To-.
(55) Fulmer, G. R.; Miller, A. J. M.; Sherden, N. H.; Gottlieb, H. E.; Nudelman, A.; Stoltz, B. M.; Bercaw, J. E.; Goldberg, K. I. NMR Chemical Shifts of Trace Impurities: Common Laboratory Solvents, Organics, and Gases in Deuterated Solvents Relevant to the Organometallic Chemist. Organometallics 2010, 29 (9), 2176–2179. https://doi.org/10.1021/om100106e.
(56) Kim, S.-T. Peptide Coupling Agents. In Encyclopedia of Toxicology; Elsevier, 2014; pp 786–787. https://doi.org/10.1016/B978-0-12-386454-3.00642-4.

(57) Han, S.-Y.; Kim, Y.-A. Recent Development of Peptide Coupling Reagents in Organic Synthesis. Tetrahedron 2004, 60 (11), 2447–2467. https://doi.org/10.1016/j.tet.2004.01.020.
(58) Lützenburg, T.; Neundorf, I.; Scholz, M. Direct Carborane-Peptide Conjugates: Synthesis and Evaluation as Non-Natural Lipopeptide Mimetics. Chemistry and Physics of Lipids 2018, 213, 62–67. https://doi.org/10.1016/j.chemphyslip.2018.03.009.
(59) Vrettos, E. I.; Sayyad, N.; Mavrogiannaki, E. M.; Stylos, E.; Kostagianni, A. D.; Papas, S.; Mavromoustakos, T.; Theodorou, V.; Tzakos, A. G. Unveiling and Tackling Guanidinium Peptide Coupling Reagent Side Reactions towards the Development of Peptide-Drug Conjugates. RSC Adv. 2017, 7 (80), 50519–50526. https://doi.org/10.1039/C7RA06655D.
(60) Jiang, H.; D'Agostino, G. D.; Cole, P. A.; Dempsey, D. R. Selective Protein N-Terminal Labeling with N-Hydroxysuccinimide Esters. Methods Enzymol 2020, 639, 333–353. https://doi.org/10.1016/bs.mie.2020.04.018.
(61) Fan, J.; Toth, I.; Stephenson, R. J. Bioconjugated Materials in the Development of Subunit Vaccines. In Comprehensive Analytical Chemistry; Elsevier, 2023; Vol. 103, pp 59–103. https://doi.org/10.1016/bs.coac.2023.02.005.
(62) Pfister, D.; Morbidelli, M. Process for Protein PEGylation. Journal of Controlled Release 2014, 180, 134–149. https://doi.org/10.1016/j.jconrel.2014.02.002.
(63) Valliant, J. F.; Guenther, K. J.; King, A. S.; Morel, P.; Schaffer, P.; Sogbein, O. O.; Stephenson, K. A. The Medicinal Chemistry of Carboranes. Coordination Chemistry Reviews 2002, 232 (1–2), 173–230. https://doi.org/10.1016/S0010-8545(02)00087-5.
(64) Carboranes Building Blocks for Materials and Ligand Development.
(65) Presolski, S. I.; Hong, V. P.; Finn, M. G. Copper-Catalyzed Azide-Alkyne Click Chemistry for Bioconjugation. Curr Protoc Chem Biol 2011, 3 (4), 153–162. https://doi.org/10.1002/9780470559277.ch110148.

Appendices

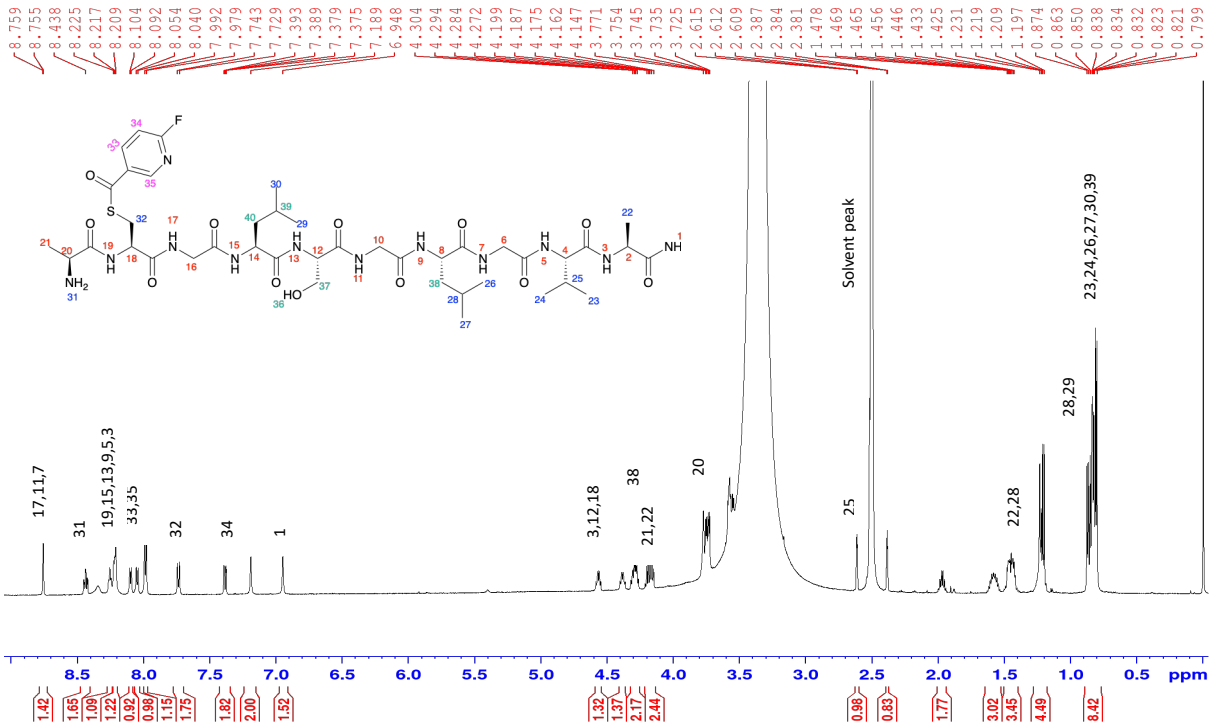

Figure1: *[1]HNMR spectrum of FNA-S-ACooP*

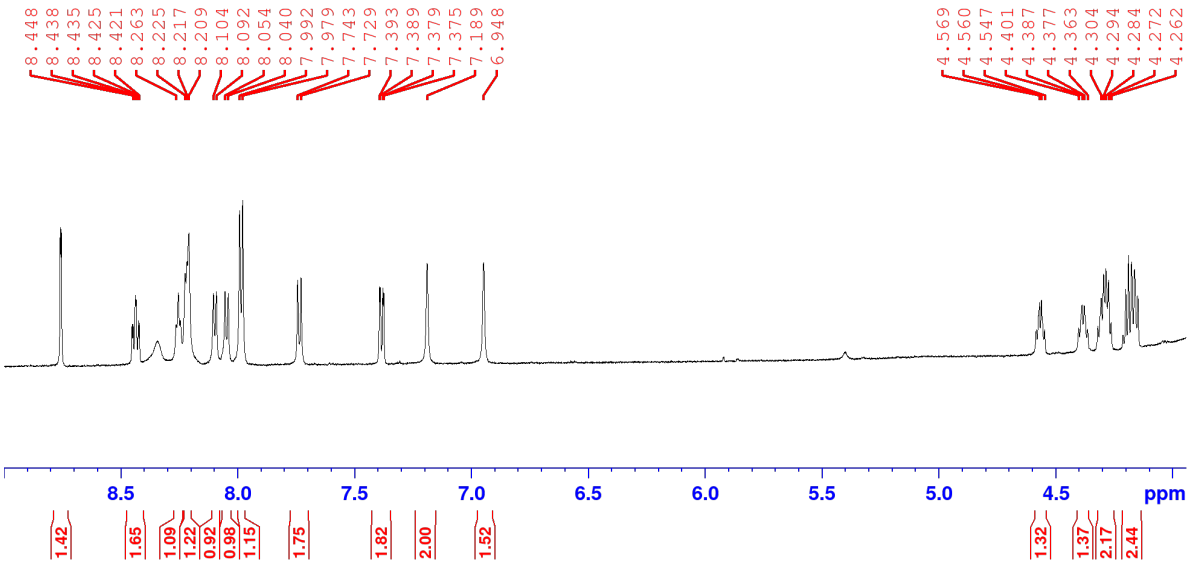

Figure 2: *Extraction from figure 1; [1]HNMR spectrum of FNA-S-ACooP* δ 4.0 ppm – 9.0 ppm

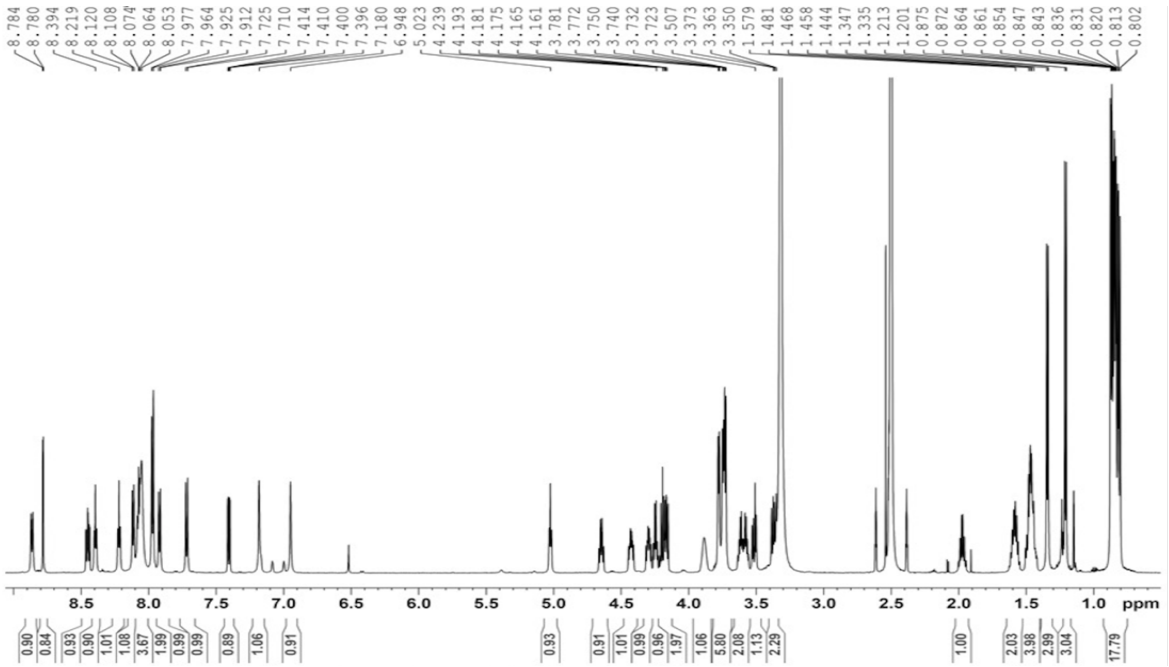

Figure 3: *^{1}HNMR spectrum of in-house made [^{18}F]FNA-S-ACooP as a reference*

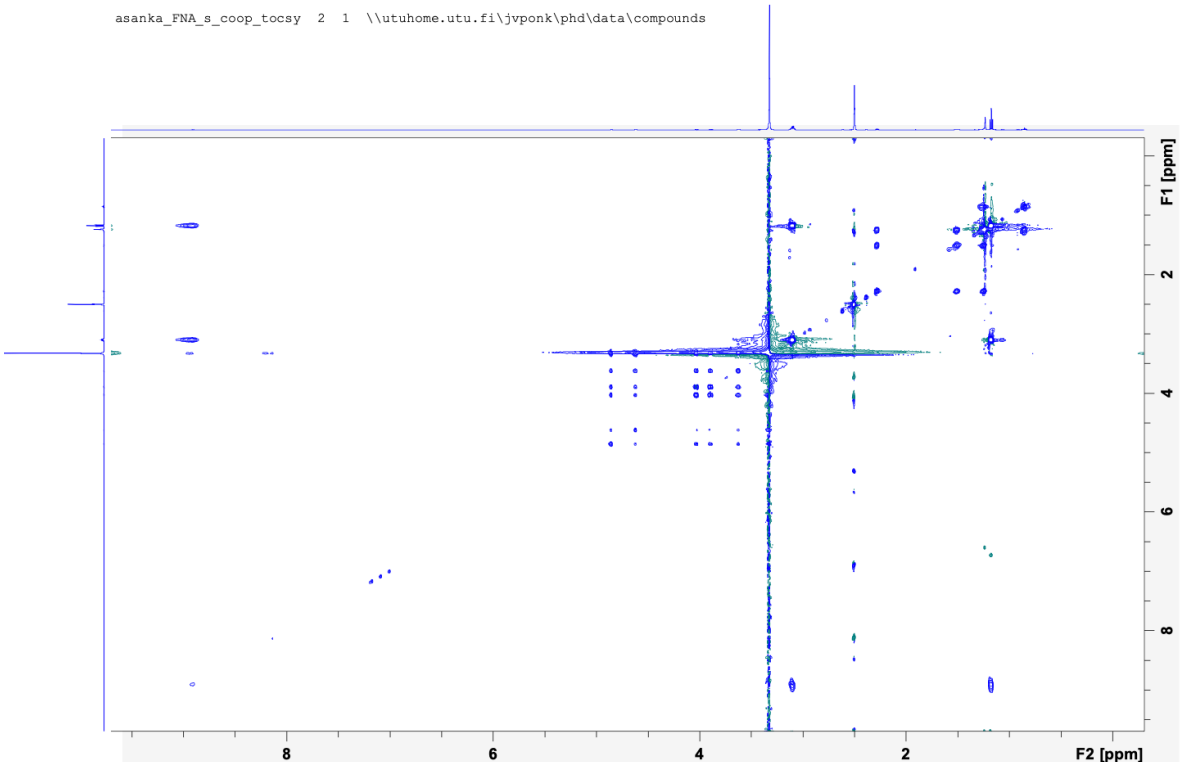

Figure 4: *TOCSY spectrum of FNA-S-ACooP*

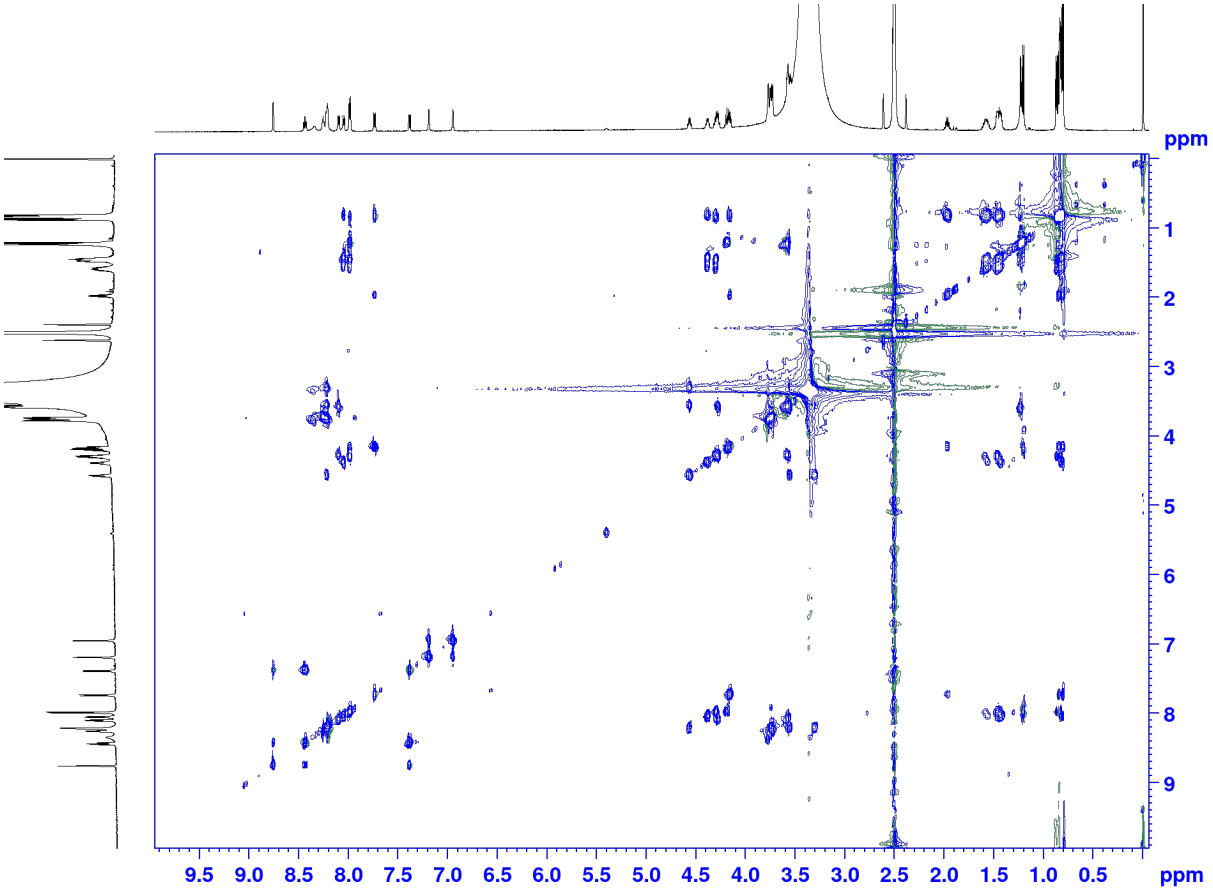

Figure 5: *TOCSY spectrum of in-house made [^{18}F] FNA-S-ACooP as a reference*

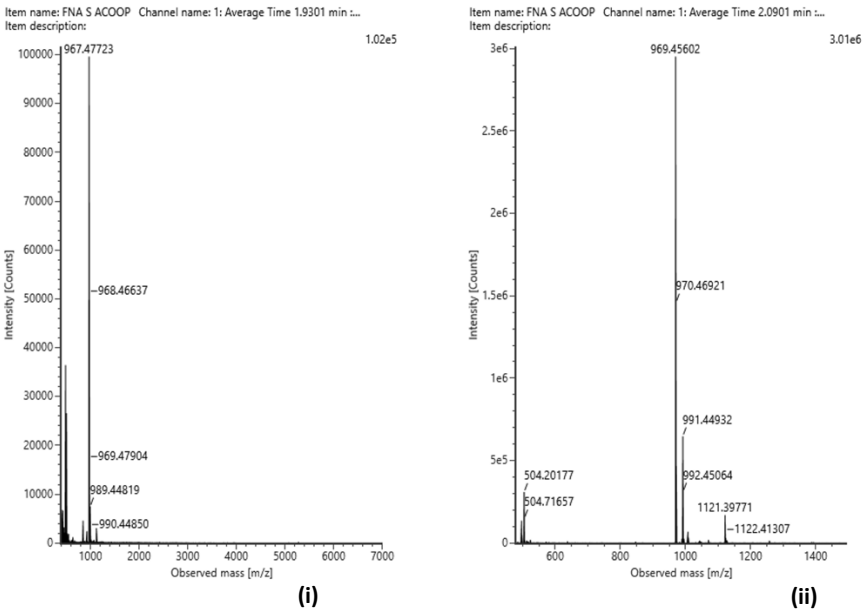

Figure 6: (i) *HRMS spectra of FNA-S-ACooP purified with TFA showing a major chromatographic peak at retention time of t_R = 2.09 minutes and* ***(ii)*** *retention time of t_R = 1.93 minutes*

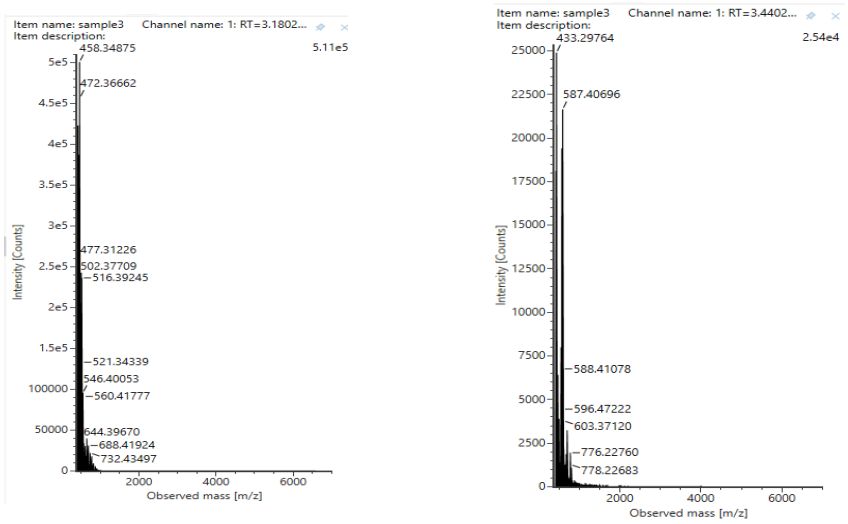

Figure 7:(i) *MS spectra of carborane-N-FNA-S-ACooP at retention time t_R = 3.18 min;* ***(ii)*** *MS spectra of carborane-N-FNA-S-ACooP at retention time t_R = 3.44 min*

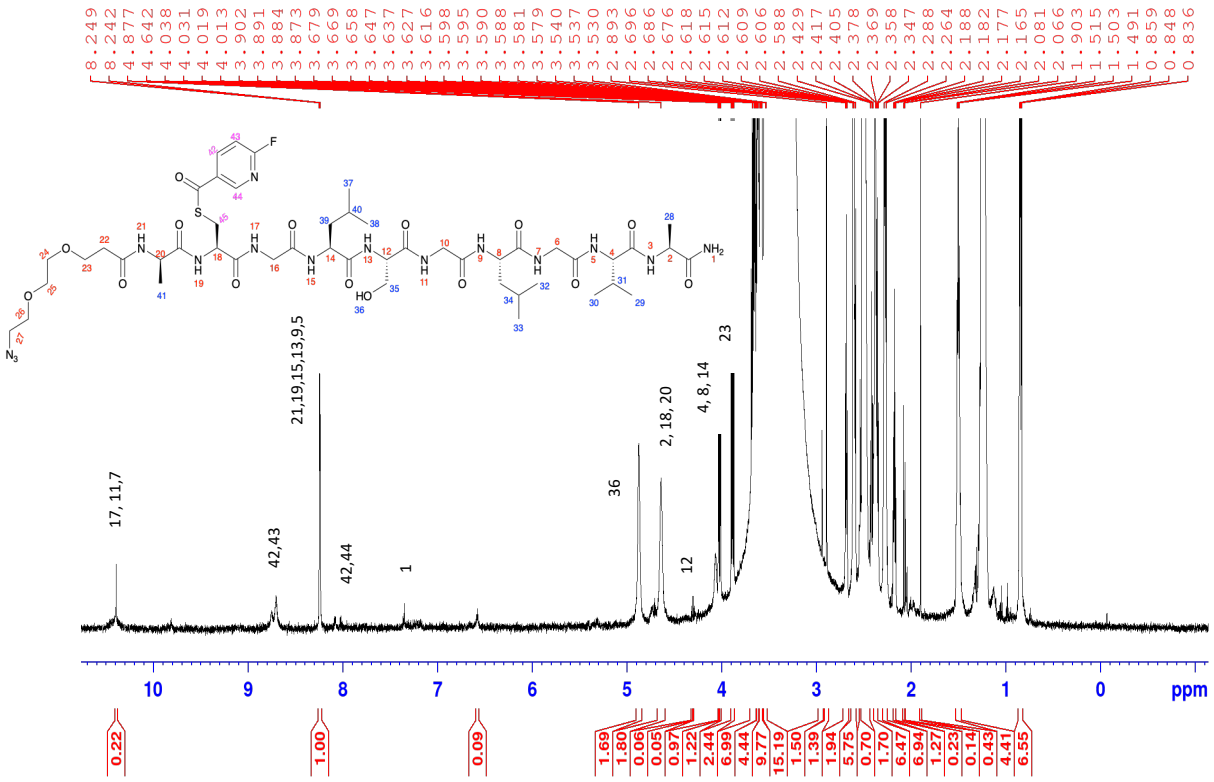

Figure 8: *^{1}HNMR spectrum of FNA-S-ACooP- N-PEG$_2$-N*

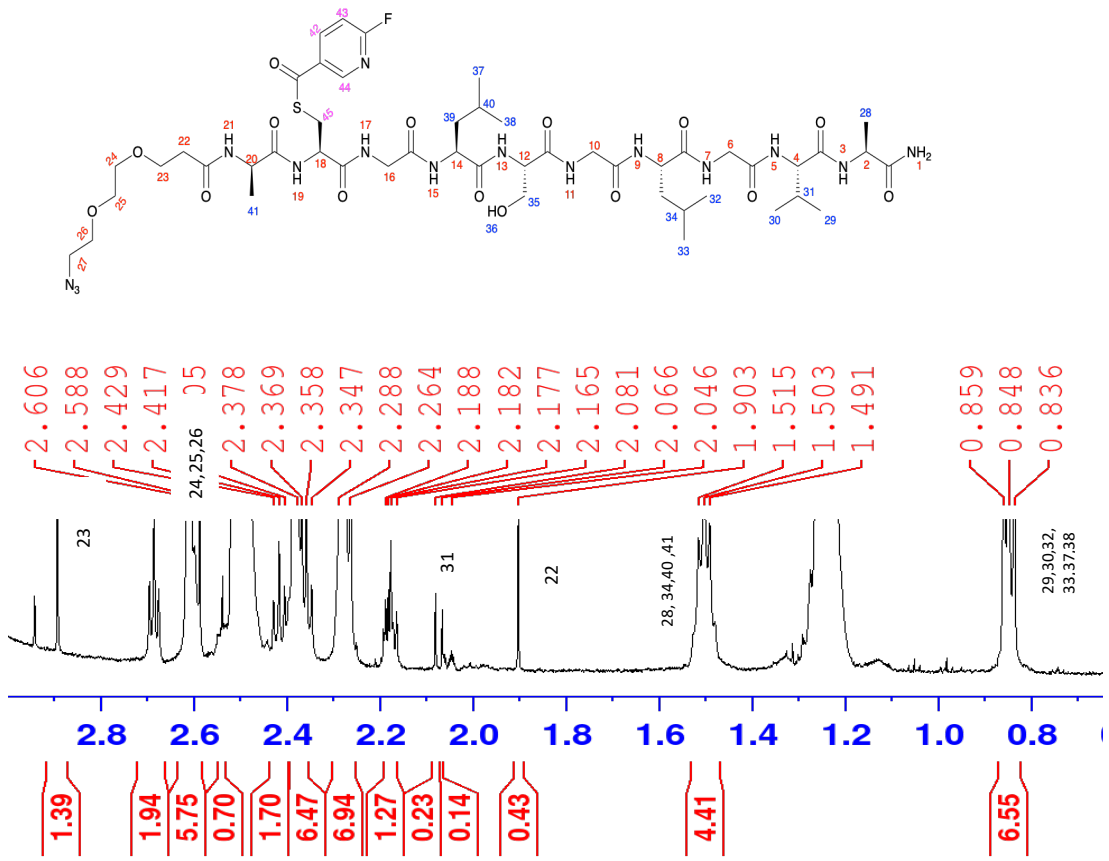

Figure 8: *Extraction from figure 6; ^{1}HNMR spectrum of FNA-S-ACooP- N-PEG$_2$-N$_3$* δ 0.8 ppm – 2.8 ppm

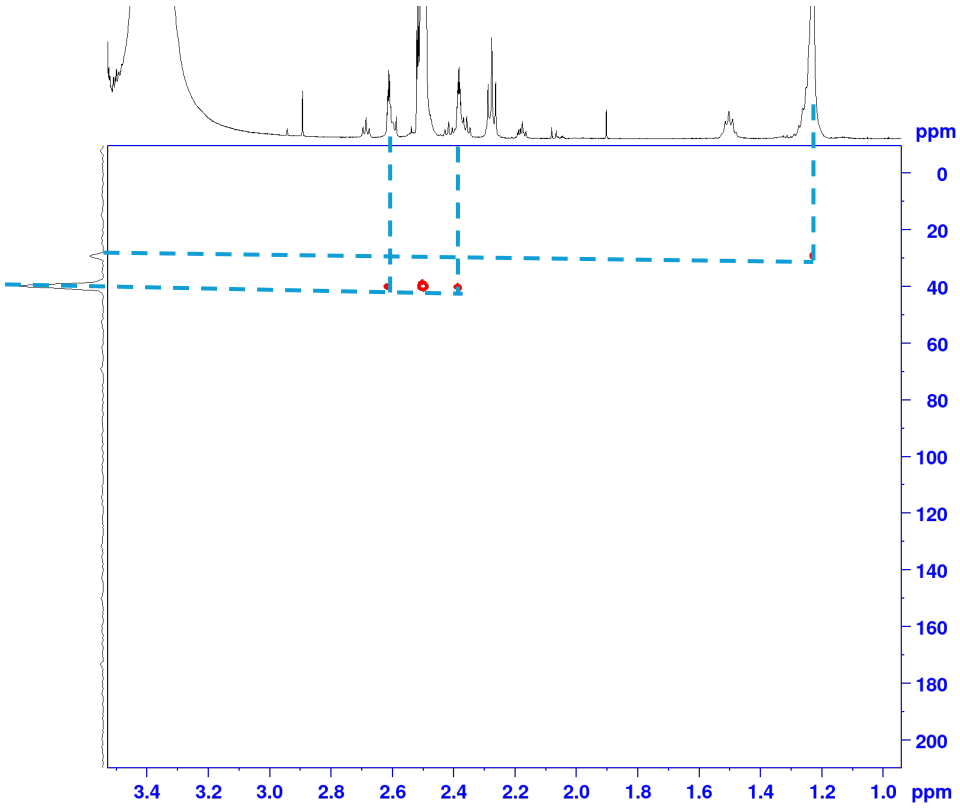

Figure 9: *HSQC spectrum of FNA-S-ACooP- N-PEG$_2$-N$_3$*